

Maximum Likelihood Estimation of Spatially Varying Coefficient Models for Large Data with an Application to Real Estate Price Prediction

Jakob A. Dambon^{*}^{1,2}, Fabio Sigrist[†]², and Reinhard Furrer[‡]^{1,3}

¹*Department of Mathematics, University of Zurich*

²*Institute of Financial Services Zug, Lucerne University of Applied Sciences and Arts*

³*Department of Computational Science, University of Zurich*

June 22, 2022

Abstract

In regression models for spatial data, it is often assumed that the marginal effects of covariates on the response are constant over space. In practice, this assumption might often be questionable. In this article, we show how a Gaussian process-based spatially varying coefficient (SVC) model can be estimated using maximum likelihood estimation (MLE). In addition, we present an approach that scales to large data by applying covariance tapering. We compare our methodology to existing methods such as a Bayesian approach using the stochastic partial differential equation (SPDE) link, geographically weighted regression (GWR), and eigenvector spatial filtering (ESF) in both a simulation study and an application where the goal is to predict prices of real estate apartments in Switzerland. The results from both the simulation study and application show that the MLE approach results in increased predictive accuracy and more precise estimates. Since we use a model-based approach, we can also provide predictive variances. In contrast to existing model-based approaches, our method scales better to data where both the number of spatial points is large and the number of spatially varying covariates is moderately-sized, e.g., above ten.

Keywords: spatial statistics, Gaussian process, covariance tapering, likelihood regularization, real estate mass appraisal

^{*}Email: jakob.dambon@math.uzh.ch, Address: Department of Mathematics, University of Zurich, Winterthurerstrasse 190, 8057 Zurich, Switzerland.

[†]Email: fabio.sigrist@hslu.ch, Address: Institute of Financial Services Zug, Campus Zug-Rotkreuz, Suurstoffi 1, 6343 Rotkreuz, Switzerland.

[‡]Email: reinhard.furrer@math.uzh.ch, Address: Department of Mathematics, University of Zurich, Winterthurerstrasse 190, 8057 Zurich, Switzerland.

1 Introduction

Over the last years, affordable measuring techniques lead to an abundance of spatial data; not only areal but in particular spatial points data. Often, the data sets contain covariates in addition to the main variable(s) of interest. These are then used in a regression model, where the goal is either predicting the response variable or inferring the relationship between the response variable and the covariates. With further advances to reduce computational cost, we are now able to analyze large spatial data sets and the literature on models and methods on how to do so is extensive. See Cressie (2011) and Heaton et al. (2019) for an overview. However, the vast majority of models assumes that covariate effects are constant over space which is not necessarily plausible.

Spatially varying coefficient (SVC) models allow for marginal effects to be non-stationary over space and thus offer a higher degree of flexibility. At the same time, SVC models have the advantage that they are easily interpretable. Several methodologies and applications with SVC models have been published. To name two, *geographically-weighted regression (GWR)* by Fotheringham et al. (2002) and a Bayesian framework with *SVC processes* by Gelfand et al. (2003) are prominent examples. An application that uses both methodologies can be found in Wheeler and Waller (2009) who model crime records in Houston, Texas. A further comparison of GWR and SVC processes is given by Finley (2010) on ecological data. It is shown that SVC processes generally have better predictive performance.

However, when it comes to estimating SVC models on large data, most of the established methodologies run into problems. Currently available implementations of Bayesian approaches such as *Gaussian predictive processes* presented in Banerjee et al. (2008) or *Gaussian Markov random field* approximations by Lindgren et al. (2011) are either limited by the number of SVCs within a model or the number of observations. This also holds true for the before mentioned SVC processes by Gelfand et al. (2003). Finally, GWR lacks a statistical sound definition and should be regarded as a purely exploratory tool. Therefore, a geostatistical estimation and prediction method is needed that, on the one hand, can deal with large number of observations and, on the other hand, can be applied to models including many SVCs.

The outline of this article is as follows: In the next section, we introduce the data set and give a first exploratory analysis that motivates the usage of SVC models. In Section 3 we formally define SVC models and give an overview of existing methods. We motivate our approach by listing potential shortcomings of the existing methods. In Section 4 we describe our *maximum likelihood estimation (MLE)* method in detail. Section 5 compares the existing methods to MLE in a large simulation study on synthetic data. A further comparison on the real data set is given in Section 6. We summarize our findings in Section 7.

2 Data Set

The data set provided by Fahlränder Partner (Zurich, Switzerland) consists of apartment transactions in Switzerland containing the selling price, six covariates and approximate coordinates for each transaction. The goal is to regress the selling price on the given covariates. An overview and description of the data is given in Table 1.

The Swiss banking secrecy prevents disclosing the exact locations of the apartments. That is why the locations are aggregated on fairly small cells and the observation locations

Table 1: Overview of the response, covariates and coordinates in our data set. There are 24,816 transaction records in total.

Name	Description	Range
Price	Transaction amount in Swiss Francs (CHF)	$60 \times 10^3 - 7,500 \times 10^3$
Area	Area in square meters	20 – 310
Year of construction	Apartments build before 1920 are set to 1920.	1920 – 2017
Micro location rating	Rating of the location on small scale, i.e. walking distance (higher meaning better)	1 – 5
Standard rating	Rating of standard of the apartment (higher meaning better)	1 – 5
Renovation rating	Need for renovation (lower meaning better)	0 – 4
Date	Quarter in which the transaction took place	Q3 2015 – Q4 2017
Easting		$200 \times 10^3 - 800 \times 10^3$
Northing		$100 \times 10^3 - 400 \times 10^3$

are represented by the cells’ centroids. The easting and northing of these centroids are given in the *LV03* coordinate reference system and their corresponding units are meters (Federal Office of Topography *swisstopo*, 1900). In total, Switzerland is divided into 5,379 of these areas of sizes ranging from 3.68 to 59,988.20 acres (0.015 to 242.764 km²), the median being 872.49 acres (3.531 km²). The smallest cells are usually being used in highly populated areas, while the larger cells are used in more rural areas.

2.1 Motivation and Exploratory Analysis

In real estate mass appraisal, there are several works that investigate or model non-stationary covariates effects. Gelfand et al. (2003) used a Bayesian SVC model with coefficients defined as *Gaussian processes (GP)* to model single-family houses in Baton Rouge, Louisiana. A frequently used tool to investigate the hypothesis of SVC in an exploratory manner is *geographically weighted regression (GWR)*. For instance, van Eggermond et al. (2011) and Cao et al. (2019) show that the coefficients of the floor level and the distance to a central business district are spatially varying. We use these findings to motivate a first exploratory analysis of the real estate data set at hand. A visual inspection of the SVCs is challenging since the underlying effects are not directly observable and first require a definition of a regression model.

With the transaction price (**price**) as a variable of interest we use the area (**area**), micro location rating (**micro**), and standard rating (**stand**) for a simple, first model. Specifically, we natural logarithm transform the price and area variables as one usually does in a hedonic model (Malpezzi, 2008; Wheeler et al., 2014). Using the R package **spgwr** by Bivand and Yu (2017), the model is fitted on the whole data set and the estimated SVCs are depicted in Figure 1.

A visual inspection of the GWR-estimated coefficients indicates that we have indeed

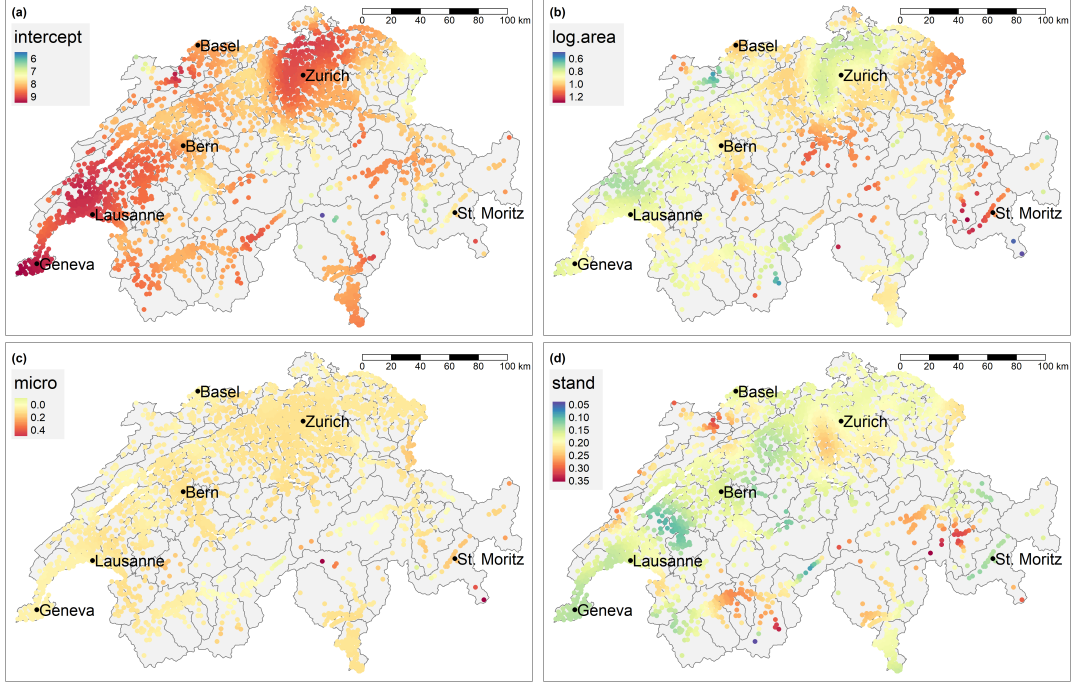


Figure 1: GWR-estimated SVCs of a model regressing the `log price` on (a) an intercept, (b) `log area`, (c) `micro`, and (d) `stand`. We are using a bandwidth of 10 km.

spatially varying coefficients. In facet (a) the intercept’s SVC is given. As expected, we see a relatively large variation in the intercept. Further, we also observe spatial variability in the area and standard effects. However, some of the effects are not in line with prior expectation as, for instance, we would expect a higher area effect in city centers. Further, the intercept and the area effect appear negatively correlated. In fact, multicollinearity is a potential drawback of GWR, see Wheeler and Tiefelsdorf (2005).

Yet, applications in context of real estate pricing like Cao et al. (2019) as well as Geng et al. (2011) report a substantial increase in R^2 by 0.19 and 0.23, respectively, compared to an OLS-based regression. We were able to observe an increase in R^2 of similar magnitude when going from an OLS to an GWR estimation. This ambiguity between, on the one hand, the quality of the estimated SVC and, on the other hand, the goodness of fit underlines the need for a statistical sound methodology for SVC models which can be applied to large data.

3 SVC Models

SVC models extend the linear regression model

$$y_i = \beta_1 x_i^{(1)} + \dots + \beta_p x_i^{(p)} + \varepsilon_i, \quad \varepsilon_i \stackrel{\text{iid}}{\sim} \mathcal{N}(0, \tau^2), \quad (1)$$

where $i = 1, \dots, n$ are the observations and p is the number of coefficients. By allowing the coefficients to vary spatially, the model equation changes to

$$y_i = \beta_1(s_i) x_i^{(1)} + \dots + \beta_p(s_i) x_i^{(p)} + \varepsilon_i, \quad \varepsilon_i \stackrel{\text{iid}}{\sim} \mathcal{N}(0, \tau^2),$$

where $s_i \in D \subset \mathbb{R}^d, d \geq 1$, denotes the location of observation i in a domain D . Here, we will work with $d = 2$. The exact specifications for the coefficients $\beta_j(\cdot)$ have yet to be defined.

3.1 Existing SVC Methods

We will give an overview of the most common methods that allow us to make inference for SVC models.

Geographically Weighted Regression (GWR) This method is widely used in practice as it is easy to implement and relatively fast in computation. It assumes model equation (1) and estimates the coefficients for each location as a weighted regression specific to that location. GWR is fully described in Fotheringham et al. (2002). As mentioned before, multicollinearity issues with local regressions are raised in Wheeler and Tiefelsdorf (2005), cf. Figure 1. A further concern is that GWR assumes that all coefficients have the same bandwidth, i.e., range. This method is readily available for R (package `spgwr` Bivand and Yu, 2017) and arcGIS (Environmental Systems Research Institute (ESRI), 2020).

Eigenvector Spatial Filtering (ESF) This method is also known as *Moran's Eigenvector Mapping (MEM)* (Griffith, 2011; Dray et al., 2006). In Murakami and Griffith (2015) it has been extended to random effects and thus is now capable of dealing with SVC models. It is readily available in the R package `spmoran` (Murakami, 2018).

The following methods are based on a model assumption where the SVC are defined with Gaussian processes (GP). That is,

$$\beta_j(\cdot) \sim \mathcal{GP}(\boldsymbol{\mu}_j(\cdot), c^{(j)}(\cdot, \cdot; \boldsymbol{\theta}_j)), \quad (2)$$

for some choice of covariance function $c^{(j)}$ with parameter vector $\boldsymbol{\theta}_j$. The covariance function works on the distances r between observation locations defined by some norm. Here we use the Euclidean norm $\|\cdot\|$. We denote $\boldsymbol{\Sigma}^{(j)}$ the covariance matrix defined as

$$(\boldsymbol{\Sigma}^{(j)})_{kl} := c^{(j)}(\underbrace{\|s_k - s_l\|}_{=r}; \boldsymbol{\theta}_j). \quad (3)$$

One of the most commonly used classes of covariance functions is the Matérn covariance function class. For a *marginal variance* σ^2 and a *range parameter* ρ , we define the Matérn covariance function $c_\nu(\cdot; \rho, \sigma^2) : [0, \infty) \rightarrow \mathbb{R}^+$ as

$$c_\nu(r; \rho, \sigma^2) = \sigma^2 \frac{2^{1-\nu}}{\Gamma(\nu)} \left(\sqrt{2\nu} \frac{r}{\rho} \right)^\nu K_\nu \left(\sqrt{2\nu} \frac{r}{\rho} \right), \quad (4)$$

where $\nu \in \mathbb{R}^+$ is the *smoothness*, r is a distance, and K_ν is the modified Bessel function of the second kind and order ν . Coming back to our assumption (2), i.e., that each SVC is modelled by a GP, this implies that each SVC is described by the covariance parameters $\boldsymbol{\theta}_j$ that consists of a variance σ_j^2 and range ρ_j , while in this paper we assume the smoothness ν_j to be known.

Bayesian SVC Processes Gelfand et al. (2003) introduced a Bayesian SVC model. It allows for prior-dependence of the coefficient processes but assumes an equal range parameter for all coefficients, i.e., $\rho_j \equiv \rho, \forall j$. The method is implemented for example in the R package `spTDyn` (Bakar et al., 2016). However, the package does not scale to large data.

Gaussian Markov Random Fields using an SPDE Link One can define a Bayesian SVC model using the link between Gaussian Markov random fields (GMRF, see Rue and Held, 2005) and GP via a stochastic partial differential equation (SPDE, see Lindgren et al., 2011). However, this SPDE link only exists for a limited number of Matérn class covariance functions. Estimation can be done using *integrated nested Laplacian approximations (INLA)* based on Rue et al. (2009) which is available in the R package INLA (www.r-inla.org, Lindgren and Rue, 2015). Due to its widely accommodated models, INLA has become quite popular over the last couple of years and is used in environmental sciences and climatology as it can deal with big data sets. A drawback of INLA is the critical assumption on the number of hyperparameters that one can estimate which should be “small, typically 2 to 5, but not exceeding 20” (Rue et al., 2017) and therefore the number of SVC in a model is limited.

Remark (SPDE link in INLA). *In the current version of INLA (version 19.09.03), the SPDE link is defined for the fractional operator order $\alpha \in (0, 2]$. In d dimensions, the relation between the fractional operator order α and the Matérn smoothness parameter ν is $\alpha = \nu + d/2$. In our case ($d = 2$) the link exists for Matérn covariance functions with smoothness $\nu \in (0, 1]$.*

Finally, we want to mention a recent proposal named spatial homogeneity pursuit of regression coefficients by Li and Sang (2019). *Spatially clustered coefficient (SCC)* models are a sub-class of SVC models. While general SVC models usually assume (smooth) spatial variation, SCCs are defined with constant patches and discontinuities in their coefficients. Li and Sang (2019) use minimum spanning trees – a method from graph theory – to model these SCCs.

3.2 Challenge

Our data model (see below in Section 6.1) contains $p = 8$ SVCs and about $n = 15,000$ observations. While the sample size itself poses no computational problems for existing geostatistical approaches for large data, the combination of the sample size and the number of SVC is challenging. In particular, when applying existing statistical SVC approaches such as in e.g. Gelfand et al. (2003) or Franco-Villoria et al. (2019) to this data, one currently runs into a computational bottleneck. This highlights the need for a statistical methodology that can deal with large data for SVC models.

4 Method: Maximum Likelihood Estimation for SVC Models

In this section, we present the SVC model we use and show how it can be estimated using MLE. We provide novel proposals on how to deal with large data as well as regularization options that help to alleviate correlation among hyper-parameters. Finally, we show how to give predictions once the model has been estimated.

4.1 Gaussian Process-based SVC Model

For each covariate j we assume that the associated coefficient $\beta_j(\cdot)$ is separated into a fixed and a random effect. That is, $\beta_j(\cdot) = \mu_j + \eta_j(\cdot)$ for some constant μ_j and a zero-mean

GP $\eta_j(\cdot)$ with a stationary covariance function $c^{(j)}$ similarly to (2), i.e.,

$$\eta_j(\cdot) \sim \mathcal{GP}(\mathbf{0}, c^{(j)}(\cdot; \boldsymbol{\theta}_j)). \quad (5)$$

We denote by $\mathbf{X} \in \mathbb{R}^{n \times p}$ the data matrix defined as $(\mathbf{X})_{ij} := x_i^{(j)}$, i.e., the i th observation of the j th covariate. The fixed effect part is given by $\mathbf{X}\boldsymbol{\mu}$, where $\boldsymbol{\mu} := (\mu_1, \dots, \mu_p)^\top \in \mathbb{R}^p$.

Let $\{s_i\}_{i=1, \dots, n}$ be not necessarily distinct observation locations. Using (3) and (5), $\boldsymbol{\eta}_j := (\eta_j(s_1), \dots, \eta_j(s_n))^\top \in \mathbb{R}^n$ is normally distributed as

$$\boldsymbol{\eta}_j \sim \mathcal{N}_n(\mathbf{0}_n, \boldsymbol{\Sigma}^{(j)}).$$

The assumption of mutual prior independence of the GPs, i.e., of $\boldsymbol{\eta}_j$, results in $\boldsymbol{\eta} := (\boldsymbol{\eta}_1, \dots, \boldsymbol{\eta}_p)^\top \in \mathbb{R}^{np}$ having the joint distribution $\boldsymbol{\eta} \sim \mathcal{N}_{np}(\mathbf{0}_{np}, \boldsymbol{\Sigma}_\eta)$ with joint covariance matrix

$$\boldsymbol{\Sigma}_\eta := \text{diag}(\boldsymbol{\Sigma}^{(1)}, \dots, \boldsymbol{\Sigma}^{(p)}). \quad (6)$$

Further, we denote by $\mathbf{W} \in \mathbb{R}^{n \times (np)}$ a sparse matrix defined as

$$\mathbf{W} := (\text{diag}(\mathbf{x}^{(1)}) \mid \dots \mid \text{diag}(\mathbf{x}^{(p)})).$$

Using this notation, the random effect part is given by $\mathbf{W}\boldsymbol{\eta}$. With the identity matrix \mathbf{I}_n , the error term is distributed as $\boldsymbol{\varepsilon} \sim \mathcal{N}_n(\mathbf{0}_n, \tau^2 \mathbf{I}_n)$ and is independent of $\boldsymbol{\eta}$. In summary, writing the response as an n -dimensional vector \mathbf{Y} , we obtain the GP-based SVC model

$$\mathbf{Y} = \mathbf{X}\boldsymbol{\mu} + \mathbf{W}\boldsymbol{\eta} + \boldsymbol{\varepsilon}. \quad (7)$$

4.2 Likelihood and Optimization

In the following, we derive the log-likelihood (LL) function for the GP-based SVC model as given in (7). The distribution of the response variable is given by

$$\mathbf{Y} \sim \mathcal{N}_n(\mathbf{X}\boldsymbol{\mu}, \boldsymbol{\Sigma}_\mathbf{Y} := \mathbf{W}\boldsymbol{\Sigma}_\eta\mathbf{W}^\top + \tau^2 \mathbf{I}_n).$$

Given the observed data, the log-likelihood function depends on the covariance parameters $\boldsymbol{\theta} := (\rho_1, \sigma_1^2, \dots, \rho_p, \sigma_p^2, \tau^2)$ as well as the mean parameters $\boldsymbol{\mu}$:

$$\text{LL}_\mathbf{Y}(\boldsymbol{\theta}, \boldsymbol{\mu}) = -\frac{1}{2} \left(\log((2\pi)^{n/2}) + \log(\det \boldsymbol{\Sigma}_\mathbf{Y}) + (\mathbf{y} - \mathbf{X}\boldsymbol{\mu})^\top \boldsymbol{\Sigma}_\mathbf{Y}^{-1} (\mathbf{y} - \mathbf{X}\boldsymbol{\mu}) \right).$$

Maximizing $\text{LL}_\mathbf{Y}(\boldsymbol{\theta}, \boldsymbol{\mu})$ is equivalent to minimizing the function

$$\text{n2LL}_\mathbf{Y}(\boldsymbol{\theta}, \boldsymbol{\mu}) = \log(\det \boldsymbol{\Sigma}_\mathbf{Y}) + (\mathbf{y} - \mathbf{X}\boldsymbol{\mu})^\top \boldsymbol{\Sigma}_\mathbf{Y}^{-1} (\mathbf{y} - \mathbf{X}\boldsymbol{\mu}).$$

The solution to the optimization problem

$$\arg \min_{(\boldsymbol{\theta}, \boldsymbol{\mu}) \in \boldsymbol{\Omega}} \text{n2LL}_\mathbf{Y}(\boldsymbol{\theta}, \boldsymbol{\mu})$$

with $\boldsymbol{\Omega} := (0, \infty)^{2p+1} \times \mathbb{R}^p \subset \mathbb{R}^{3p+1}$ cannot be computed analytically and one relies on numerical optimization. We use the quasi Newton method "L-BFGS-B" by Byrd et al. (1995) implemented in the R function `optim` to numerically minimize $\text{n2LL}_\mathbf{Y}$. This optimization approach repeatedly requires the computation of $\boldsymbol{\Sigma}_\mathbf{Y}$ with updated parameters $\boldsymbol{\omega}$ and subsequently computing both the determinant and the inverse of $\boldsymbol{\Sigma}_\mathbf{Y}$. Both of these tasks are computationally intensive.

4.2.1 Large Data

It is at this point that the computational burden of constructing Σ_Y and computing its determinant as well as its inverse becomes apparent. Recall that \mathbf{W} is a matrix of dimension $n \times (np)$ and Σ_η is of dimension $(np) \times (np)$. Using the formal definition of $\Sigma_Y = \mathbf{W}\Sigma_\eta\mathbf{W}^\top + \tau^2\mathbf{I}_n$ and the sparsity of \mathbf{W} , one can verify that the construction of Σ_Y alone using the naive matrix multiplication is of run time $\mathcal{O}(n^2p^2)$. A Cholesky-decomposition is then being used to compute both the determinant and the inverse of $n \times n$ matrix Σ_Y more efficiently. This however has also runtime $\mathcal{O}(n^3)$.

To reduce the computational load, we will exploit the mutual prior independence of the GPs. We introduce the *outer product* of a covariate $\mathbf{x}^{(j)}$ as $\mathbb{X}^{(j)} := \mathbf{x}^{(j)} (\mathbf{x}^{(j)})^\top$. This allows us to write Σ_Y using the Hadamard product (also known as the Schur or direct product) \odot as:

$$\Sigma_Y = \left(\sum_{j=1}^p \Sigma^{(j)} \odot \mathbb{X}^{(j)} \right) + \tau^2 \mathbf{I}_n. \quad (8)$$

Therefore, we do not have to compute the full matrix multiplication $\mathbf{W}\Sigma_\eta\mathbf{W}^\top$ and the runtime for the construction of (8) is $\mathcal{O}(n^2p)$. To reduce the run time for the Cholesky-decomposition, we use covariance tapering proposed by Furrer et al. (2006). In this approach, we taper the covariance matrices $\Sigma^{(j)}$ by multiplying them with an appropriate compactly supported correlation matrix, say, \mathbf{C}_{ρ^*} , where ρ^* is the tapering range. Given the underlying covariance functions $c^{(j)}$, without loss of generality, one can choose one corresponding function c^* which is compactly supported on $[0, \rho^*]$ that defines the correlation matrix \mathbf{C}_{ρ^*} (Furrer et al., 2006). Then the tapered covariance matrix $\Sigma_{\text{tap}}^{(j)} := \Sigma^{(j)} \odot \mathbf{C}_{\rho^*}$ is sparse with $(\Sigma_{\text{tap}}^{(j)})_{kl} = 0$ for $\|s_k - s_l\| \geq \rho^*$. Using (8), one can easily verify that

$$\Sigma_{Y, \text{tap}} := \left(\sum_{j=1}^p \Sigma_{\text{tap}}^{(j)} \odot \mathbb{X}^{(j)} \right) + \tau^2 \mathbf{I}_n = \left(\sum_{j=1}^p \Sigma^{(j)} \odot \mathbb{X}^{(j)} \right) \odot \mathbf{C}_{\rho^*} + \tau^2 \mathbf{I}_n$$

is sparse, too.

4.2.2 ML Estimate Using Direct Optimization Procedure

Using a straightforward optimization approach the ML estimate is defined as

$$\hat{\omega}_{\text{ML}} := \arg \min_{(\boldsymbol{\theta}, \boldsymbol{\mu}) \in \Omega} \text{n2LL}_Y(\boldsymbol{\theta}, \boldsymbol{\mu}).$$

When increasing the number of SVCs p , the dimension of parameter space Ω increases and the optimization becomes computationally expensive and numerically unstable. Thus it is crucial to reduce the dimension of the parameter space Ω when working with many SVC. We solve this problem by proposing to optimize the profile likelihood in $\boldsymbol{\theta}$, which is given by:

$$\arg \min_{\boldsymbol{\theta} \in \Theta} \text{n2LL}_Y(\boldsymbol{\theta}, \hat{\boldsymbol{\mu}}_{\text{GLS}}(\boldsymbol{\theta})),$$

where $\Theta := (0, \infty)^{2p+1}$ and $\hat{\boldsymbol{\mu}}_{\text{GLS}}(\boldsymbol{\theta})$ is the generalized least squares estimator, i.e.,

$$\hat{\boldsymbol{\mu}}_{\text{GLS}}(\boldsymbol{\theta}) := (\mathbf{X}^\top \Sigma_Y^{-1}(\boldsymbol{\theta}) \mathbf{X})^{-1} \mathbf{X}^\top \Sigma_Y^{-1}(\boldsymbol{\theta}) \mathbf{y}.$$

The ML estimate is given by numerically optimizing the following:

$$\begin{aligned}\widehat{\omega}_{\text{ML}} &:= (\widehat{\theta}_{\text{ML}}, \widehat{\mu}_{\text{ML}}), \quad \text{where} \\ \widehat{\theta}_{\text{ML}} &:= \arg \min_{\theta \in \Theta} \text{n2LL}_{\mathbf{Y}}(\theta, \widehat{\mu}_{\text{GLS}}(\theta)), \\ \widehat{\mu}_{\text{ML}} &:= \widehat{\mu}_{\text{GLS}}(\widehat{\theta}_{\text{ML}}).\end{aligned}$$

4.2.3 Regularization Using PC Priors

Due to weak identifiability and posterior correlation, the optimization concerning the covariance parameters can be unstable. We want to apply some form of regularization to ensure the numerical optimization problem is well-posed. Recent advances by Simpson et al. (2017) and extensions thereof by Fuglstad et al. (2018) introduced penalizing complexity (PC) priors for Gaussian random fields of Matérn class. We use these PC priors as regularizers to construct a regularized likelihood by extending our pure likelihood or profile likelihood approach from Section 4.2.2, respectively. In the following, we will define the *regularized parameter estimate*.

In our parametrization of the Matérn covariance function and with $d = 2$, the PC priors for a single GP with range ρ and marginal standard deviation σ (Fuglstad et al., 2018, Theorem 2.6) take the form

$$\pi_{\text{PC}}(\rho, \sigma) := \lambda_{\rho} \lambda_{\sigma} (2\rho)^{-2} \exp(-\lambda_{\rho} (2\rho)^{-1} - \lambda_{\sigma} \sigma),$$

where λ_{ρ} and λ_{σ} are defined by the prior beliefs on the lower tail of the range, $\mathbb{P}(\rho < \rho_0) = \alpha_{\rho}$, and the upper tail of the standard deviation, $\mathbb{P}(\sigma > \sigma_0) = \alpha_{\sigma}$, respectively. They are given by $\lambda_{\rho} = -2 \log(\alpha_{\rho}) \rho_0$ and $\lambda_{\sigma} = -\log(\alpha_{\sigma})/\sigma_0$. Under iid assumption on each prior and some initial beliefs this defines the regularized estimate using $\text{n2LL}_{\mathbf{Y}}$ as:

$$\widehat{\omega}_{\text{reg}} := \arg \min_{(\theta, \mu) \in \Omega} \left(\text{n2LL}_{\mathbf{Y}}(\theta, \mu) + \sum_{j=1}^p \left(\frac{\lambda_{\rho_j}}{\rho_j} + 4 \log \rho_j + 2 \lambda_{\sigma_j} \sigma_j \right) \right).$$

4.3 Prediction of Coefficient Processes

In the following, we describe how to predict the covariate effects at locations that possibly have not been observed, given estimated parameters $\widehat{\omega}_{\text{ML}}$. In the classical case of predicting a single GP at spatial points the *empirical best linear unbiased predictor (EBLUP)* is used (Cressie, 1990). In the case of SVCs, we likewise establish the EBLUP in the following.

We first extend our notation from observed locations $\mathbf{s} = (s_1, \dots, s_n)^{\top}$ to the n' locations we want to make predictions for, namely $\mathbf{s}' = (s'_1, \dots, s'_{n'})^{\top}$. These may or may not include already observed locations. The distributions of $\beta' := \beta(\mathbf{s}') = \mu_{\beta'} + \eta(\mathbf{s}')$ and \mathbf{Y} are again normally distributed with respective means $\mu_{\beta'} := \mu \otimes \mathbf{1}_{n'}$ and $\mathbf{X}\mu_{\beta}$. Estimating the latent coefficient processes is done in a two step approach where we first estimate $\eta' := \eta(\mathbf{s}')$ and then add the mean estimate of $\mu_{\beta'}$. We start by considering the joint distribution

$$\begin{pmatrix} \eta' \\ \mathbf{Y} \end{pmatrix} \sim \mathcal{N}_{n'p+n} \left(\begin{pmatrix} \mathbf{0}_{n'p} \\ \mu_{\mathbf{Y}} \end{pmatrix}, \begin{pmatrix} \Sigma_{\eta'} & \Sigma_{\eta'\mathbf{Y}} \\ \Sigma_{\mathbf{Y}\eta'} & \Sigma_{\mathbf{Y}} \end{pmatrix} \right).$$

The covariance matrix $\Sigma_{\boldsymbol{\eta}'}$ is defined for locations $s'_1, \dots, s'_{n'}$ in an analogous way to (3) and (6), namely $(\Sigma'^{(j)})_{kl} := c^{(j)}(\|s'_k - s'_l\|; \boldsymbol{\theta}_j)$ and hence

$$\Sigma_{\boldsymbol{\eta}'} := \text{diag}(\Sigma'^{(1)}, \dots, \Sigma'^{(p)}).$$

The covariance matrix $\Sigma_{\mathbf{Y}}$ is given in (8). The cross-covariances matrices $\Sigma_{\boldsymbol{\eta}'\mathbf{Y}}$ and $\Sigma_{\mathbf{Y}\boldsymbol{\eta}'}$ are defined as

$$\begin{aligned}\Sigma_{\mathbf{Y}\boldsymbol{\eta}'} &:= \text{Cov}(\mathbf{X}\boldsymbol{\mu} + \mathbf{W}\boldsymbol{\eta} + \boldsymbol{\varepsilon}, \boldsymbol{\eta}') = \mathbf{W}\text{Cov}(\boldsymbol{\eta}, \boldsymbol{\eta}'), \\ \Sigma_{\boldsymbol{\eta}'\mathbf{Y}} &:= \Sigma_{\mathbf{Y}\boldsymbol{\eta}'}^\top,\end{aligned}$$

where $\text{Cov}(\boldsymbol{\eta}, \boldsymbol{\eta}')$ is again defined as (3) and (6), but now with corresponding locations s_1, \dots, s_n and $s'_1, \dots, s'_{n'}$. Using the conditional distribution $\boldsymbol{\eta}'|\mathbf{Y} = \mathbf{y}$ and plugging in $\hat{\boldsymbol{\omega}}_{\text{ML}}$ one receives the EBLUP for SVC as

$$\hat{\boldsymbol{\eta}}' := \hat{\Sigma}_{\boldsymbol{\eta}'\mathbf{Y}} \hat{\Sigma}_{\mathbf{Y}}^{-1} (\mathbf{y} - \hat{\boldsymbol{\mu}}_{\mathbf{Y}})$$

and therefore $\hat{\boldsymbol{\beta}}' := \hat{\boldsymbol{\mu}}_{\boldsymbol{\beta}'} + \hat{\boldsymbol{\eta}}'$. One can then use corresponding data \mathbf{X}' and \mathbf{W}' at locations \mathbf{s}' to get predictions for \mathbf{Y}' . Predictive variances of such $\hat{\mathbf{Y}}'$ are derived in a similar way as above and given by the diagonal of $\Sigma_{\mathbf{Y}'} - \Sigma_{\mathbf{Y}'\mathbf{Y}} \Sigma_{\mathbf{Y}}^{-1} \Sigma_{\mathbf{Y}\mathbf{Y}'}$.

4.4 R package varycoef

The MLE described in this section is implemented in the R package `varycoef` (Dambon et al., 2019). It is used throughout this work whenever the MLE approach is mentioned. We indicate the usage of our method and the R package `varycoef` on GP-based SVC models by the abbreviation MLE with possible suffixes.

5 Simulation Study

This and the next section are designated to compare existing and our proposed methods in regard to parameter estimation and prediction accuracy. From Section 3.1, we exclude the Bayesian SVC processes method since it does not scale to large data. Further, since SCC and smooth SVC models are inherently different, we exclude the spatial homogeneity pursuit approach, too.

5.1 Setup

In order to empirically validate our method and to compare it to existing methods, we define the following simulation setup. We simulate $N := 100$ times a GP with varying numbers of SVCs p and sample sizes n' . Latter is defined by a positive integer q such that $n' = (2q)^2$ is the number of data points and locations which are sampled from a *perturbed grid* (Furrer et al., 2016).

A perturbed grid consists of $(2q) \times (2q)$ unit squares. For each $(r, s) \in \{0, \dots, 2q - 1\}^2$, we uniformly draw a single location from a square $[r + \delta, (r + 1) - \delta] \times [s + \delta, (s + 1) - \delta]$, where $\delta \in [0, 0.5)$ restricts a unit square area by an outer margin. Finally, we standardize the locations by $(2q)^{-1}$ such that the total domain of a perturbed grid is contained in the unit square. Thus, we receive the sample locations $s_1, \dots, s_{n'}$. An example is given in Figure 2.

At these locations the SVCs, the error term ε , and the data \mathbf{X} are sampled and we compute the response \mathbf{y} . We set $\mathbf{x}^{(1)} = \mathbf{1}_n$ which allows us to model a spatially varying intercept. The remaining data of \mathbf{X} is sampled from a standard-normal distribution for coefficients $j = 2, \dots, p$.

The data is then divided into three disjoint folds, (i) a training data set $\mathcal{S}_{\text{train}}$, (ii) a test data set for interpolation $\mathcal{S}_{\text{interpolate}}$, and (iii) a test data set for extrapolation $\mathcal{S}_{\text{extrapolate}}$. The unit square is partitioned into four quadrants. The lower right quadrant is an *extrapolation test set* and contains 25% of the data. In the other quadrants, 25% of the data is randomly assigned as *interpolation test set*. On the rest (50%) of the data, the model is being estimated. Thus, we have a partition:

$$\mathcal{S} := \mathcal{S}_{\text{train}} \cup \mathcal{S}_{\text{interpolate}} \cup \mathcal{S}_{\text{extrapolate}} = \{1, \dots, n'\},$$

$$n := |\mathcal{S}_{\text{train}}| = \frac{n'}{2}, \quad |\mathcal{S}_{\text{interpolate}}| = |\mathcal{S}_{\text{extrapolate}}| = \frac{n'}{4}.$$

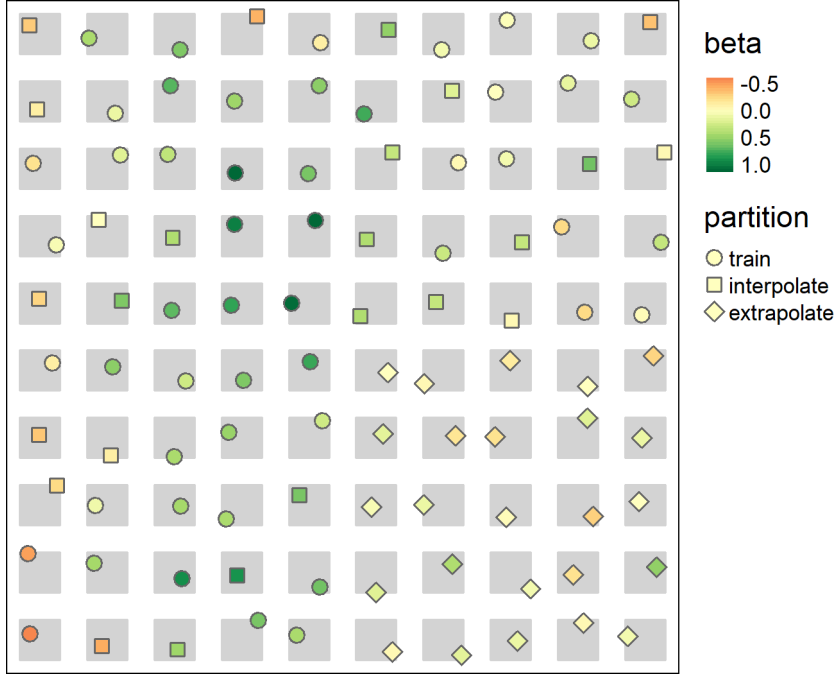


Figure 2: Example of a perturbed grid defined with $q = 5$ for $n' = 100$ sample locations and a partition into training, interpolation, and extrapolation testing. The grey patches are the sampling domain. The distance between each patch is at least δ/q . Here and in all of our simulations, δ is set to 0.2.

In total, there are three simulation settings which differ in the number of total sampled points n' and SVCs p and five methods for SVC modeling, see Table 2 for an overview. The MLE methods include the optimization using the profile likelihood (MLE) and regularized profile likelihood (MLE.r). The SPDE method has been implemented with the R package INLA (Lindgren and Rue, 2015) and uses the same PC priors as MLE.r, namely $\mathbb{P}(\rho < 0.075) = 0.05$ and $\mathbb{P}(\sigma > 0.25) = 0.05$. Methods ESF and GWR are implemented with the R packages `spmoran` (Murakami, 2018) and `spgwr` (Bivand and Yu, 2017), respectively. The superscript *tap* in Table 2 indicates covariance tapering for MLE, since Simulation 2 has the most observations. The taper range ρ^* is 0.2. Due to the number of SVCs, the SPDE method cannot be applied on Simulation 2, hence the cross mark in Table 2.

Table 2: Overview of simulations and methods.

	Simulations		
	1	2	3
n'	2,500	10,000	2,500
n	1,250	5,000	1,250
p	3	3	10
Methods			
MLE	✓	✓ ^{tap}	✓
MLE.r	✓	✓ ^{tap}	✓
SPDE	✓	✓	✗
ESF	✓	✓	✓
GWR	✓	✓	✓

In each repetition $w = 1, \dots, N$ and for each method m , we calculate the RMSE between the estimated SVC $\widehat{\beta}_j^{(m,w)}$ and the true SVC β_j in each fold

$$\kappa \in \{\text{train}, \text{interpolate}, \text{extrapolate}\}.$$

Analogously, we calculate the RMSE for the response. Thus, we have:

$$\text{RMSE}_{\kappa}^{(m,w)}(\beta_j) = \sqrt{\frac{1}{|\mathcal{S}_{\kappa}|} \sum_{i \in \mathcal{S}_{\kappa}} \left| \beta_j(s_i) - \widehat{\beta}_j^{(m,w)}(s_i) \right|^2}, \quad (9)$$

$$\text{RMSE}_{\kappa}^{(m,w)}(\mathbf{y}) = \sqrt{\frac{1}{|\mathcal{S}_{\kappa}|} \sum_{i \in \mathcal{S}_{\kappa}} |y(s_i) - \widehat{y}^{(m,w)}(s_i)|^2}. \quad (10)$$

In all of our simulation studies we assume the type of covariance function to be known, which is why we have to define it here. Since we expect in most of our applications the fields to be not too smooth, we follow the recommendation of Stein (1999) and use exponential covariance functions. The exponential covariance function is a special case of the Matérn class covariance functions with smoothness parameter $\nu = 1/2$, cf. (4). Thus, we have

$$(\Sigma^{(j)})_{kl} := c_{1/2}(\|s_k - s_l\|; \theta_j) = \sigma_j^2 \exp\left(-\frac{\|s_k - s_l\|}{\rho_j}\right), \quad \text{for all } j.$$

5.2 Results

5.2.1 Simulation 1: Base Setup

The base simulation setup samples $n' = 2,500$ from a perturbed grid with $p = 3$ SVCs. The parameters of the true model are provided in Table 3. The results of the parameter estimation which is available with methods MLE and SPDE are given in Figure 3. Without any regularization, there is one outlier in the estimation of the covariance parameters, namely in the range for the third SVC. With regularization, i.e., methods MLE.r and SPDE, the results are very similar. The only difference is the over estimation of the nugget variance by SPDE. Between MLE and MLE.r, one can see the regularization effect in the covariance parameter estimates. Regarding the mean effects, there is no difference

Table 3: Parameters of the underlying true model in Simulation 1 and 2.

Parameters	Effects j		
	1	2	3
μ_j	0.00	0.00	0.00
ρ_j	0.10	0.20	0.15
σ_j^2	0.20	0.10	0.05
σ_{nugget}^2	0.03		

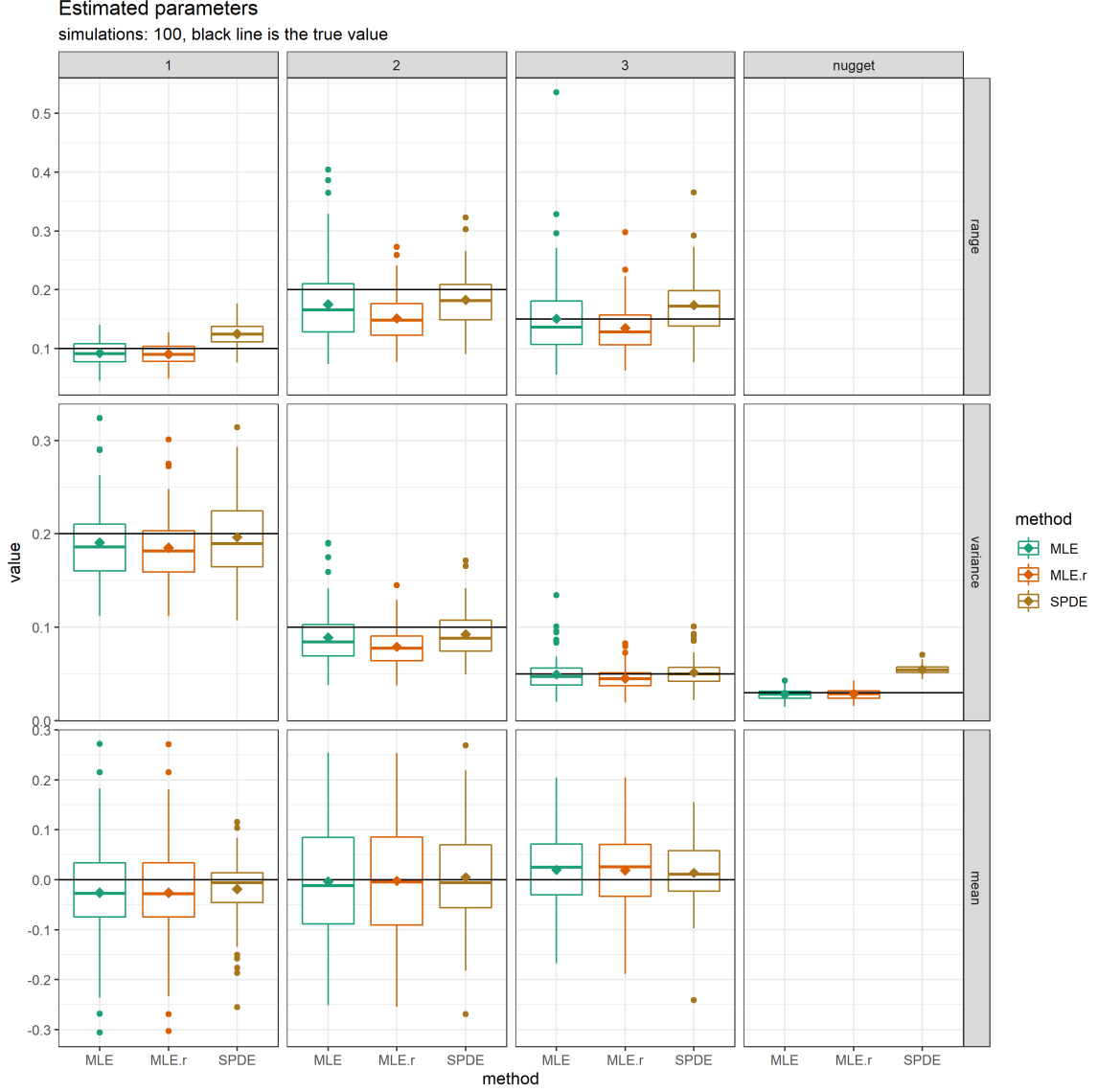


Figure 3: Estimated covariance and mean parameters of MLE and SPDE methods of Simulation 1. The box plots consists of 100 estimations of different realization. The diamonds indicate the means. True values are given by black lines.

between MLE and MLE.r. However, SPDE appears to estimate mean effects with more precision.

Across the methods MLE, MLE.r, and SPDE, the RMSE as given in (9) is very similar for all SVCs and all folds. There is a slight advantage in SVC 1 which is modeling

intercept for MLE and MLE.r compared to SPDE. This probably translates to the results for (10), i.e., the RMSE for the response. Overall, one can see that MLE, MLE.r, and SPDE are quite similar while ESF lacks behind. The results are depicted as box plots in Figure 4 for all 100 repetitions within the simulation. The results for GWR are not shown as they are far off, cf. Figure 9.

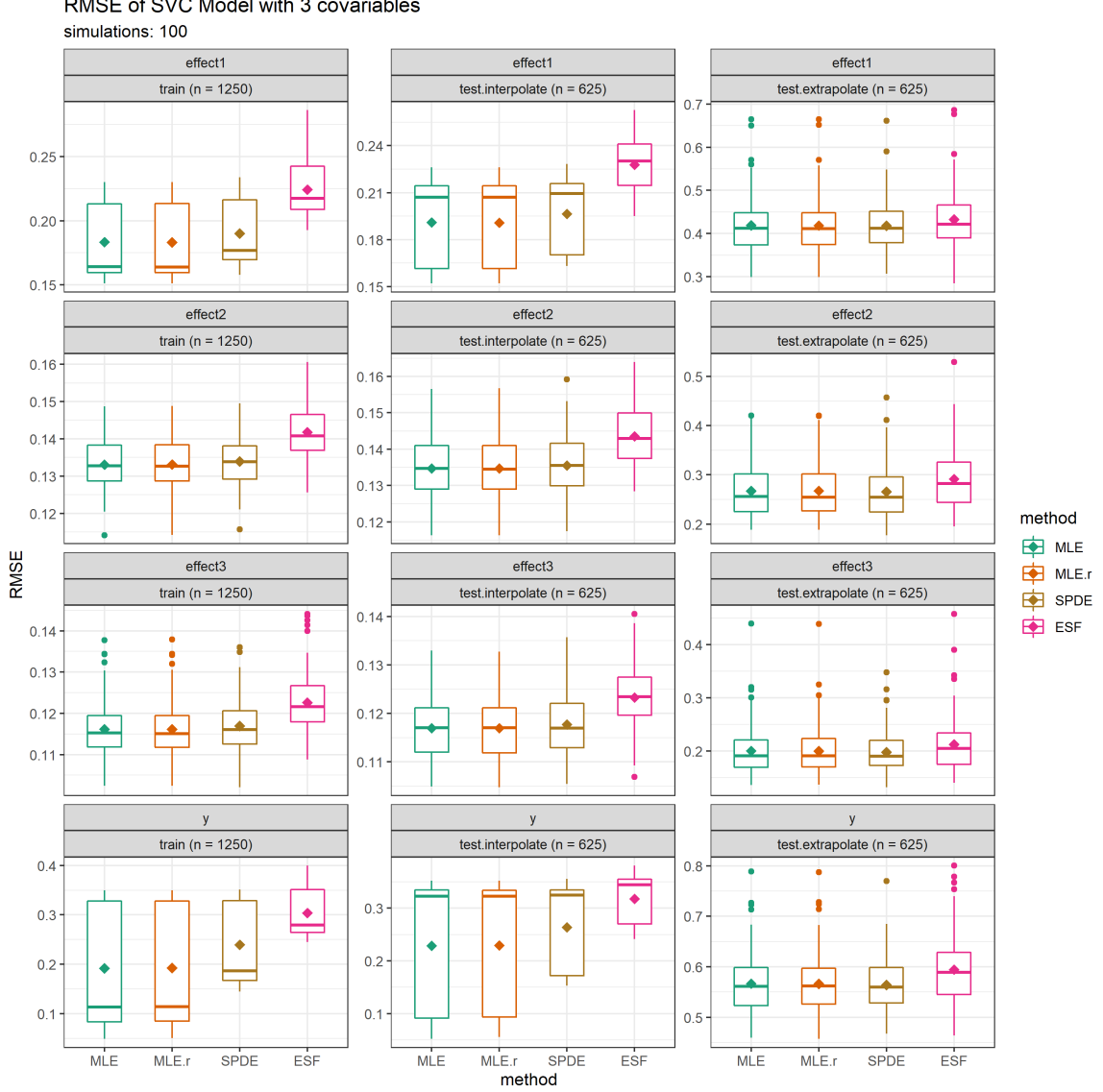


Figure 4: Box plots of RMSE between true β_j and $\hat{\beta}_j$ as well as between \mathbf{y} and $\hat{\mathbf{y}}$ for Simulation 1 in corresponding partition, see (9) and (10). The diamonds indicate the means. Note the different ranges of the y -axis.

5.2.2 Simulation 2: Number of Observations is $n' = 10,000$

Simulation 2 has the same underlying true model to simulate the data from, cf. Table 3, but using a data set with 10,000 observations. In order to allow our method to scale to data sets with a large n , we introduced covariance tapering (Furrer et al., 2006) in both MLE without and with regularization. With the introduction of a tapering range, which in this simulation study was set to $\rho^* = 0.2$, the covariance matrices become sparse.

While this has a positive impact on computation time, it results in biased estimates for the covariance parameters. Due to tapering, the ranges were overestimated by MLE and MLE.r, whilst all variances of the SVCs were underestimated. SPDE performed very similarly as in Simulation 1, cf. Figure 5. Again, we can observe that parameter estimation of MLE.r is better than MLE without regularization, cf. Figure 12 in Appendix A.2.

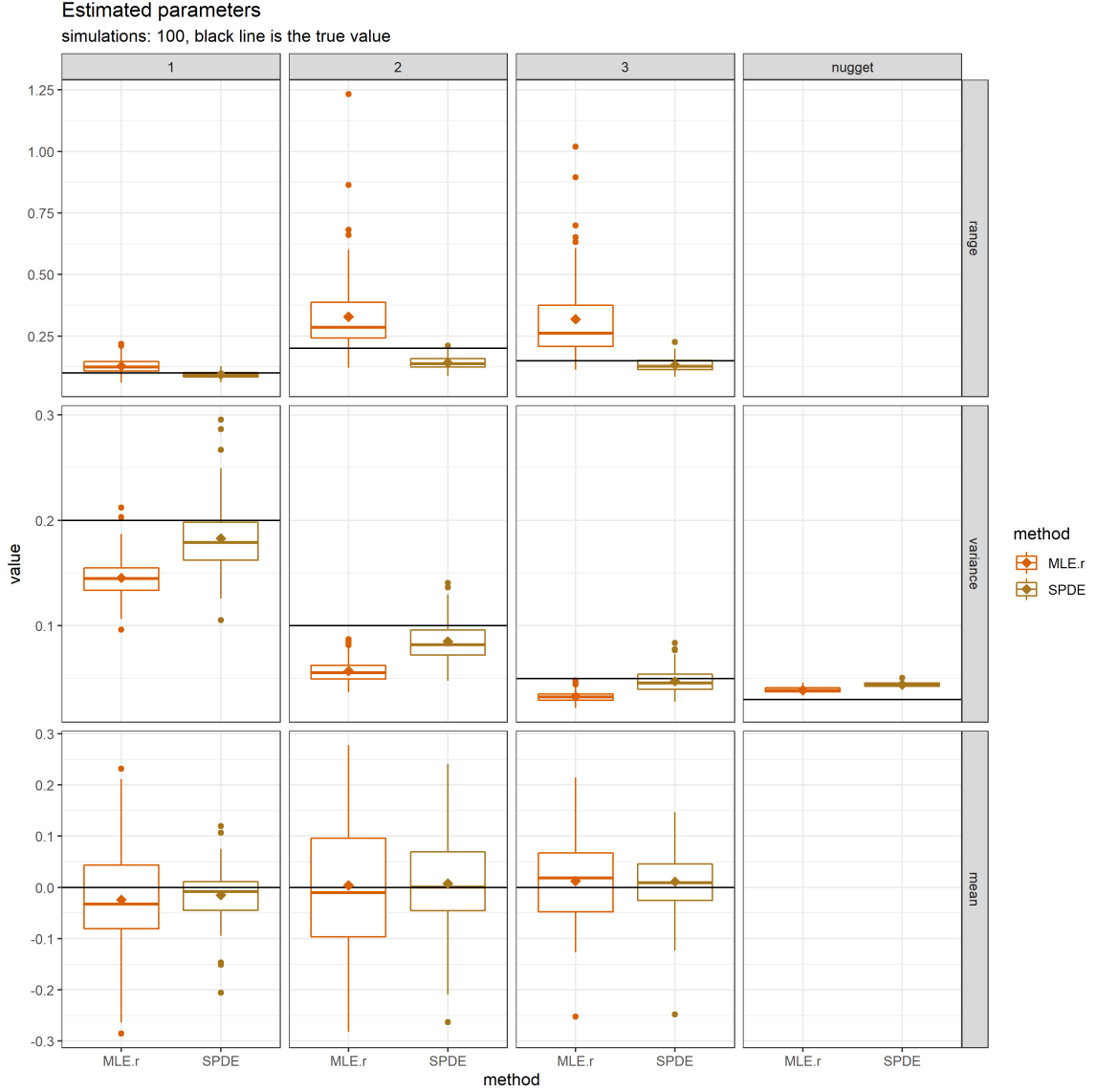


Figure 5: Box plots represent estimated covariance and mean parameters by MLE.r and SPDE methods in Simulation 2. The diamonds indicate the means. True values are given by black lines. For MLE results we refer to Figure 12 in Appendix A.2.

Further, we compute the RMSE of the estimated SVCs as given in (9) and (10). The results are depicted in Appendix A.2. They are very similar to what we observed in Simulation 1 with Figure 4 and Figure 9 in Appendix A.1. The main difference that we can see is that the MLE.r overall performs better than MLE without regularization. Hence, MLE.r surpasses MLE in both parameter estimation and SVC prediction while trailing behind SPDE under a higher number of observations.

5.2.3 Simulation 3: Number of SVCs is $p = 10$

In this simulation, we have $p = 10$ SVCs sampled from the model with the true parameters as defined in Table 4. We cannot run SPDE due to too many SVCs. Thus, MLE and MLE.r are the only methods with which we are able to estimate the parameters. The empirical results show that our ML-estimator yields unbiased results, which qualitatively are close to the results of MLE given in Figure 3. Here, we note that MLE.r outperforms MLE again. In predictive performance measured by the RMSE, the MLE and MLE.r methods are very similar and both surpass ESF. All of the results are depicted in Appendix A.3.

Table 4: Parameters of the underlying true model in Simulation 3. Compared to Simulation 1 and 2 the first SVCs are exactly defined as before. The nugget is now larger to ensure similar noise to signal ratio.

Parameters	Effects j									
	1	2	3	4	5	6	7	8	9	10
μ_j	0.00	0.00	0.00	0.00	0.00	0.00	0.00	0.00	0.00	0.00
ρ_j	0.10	0.20	0.15	0.10	0.05	0.05	0.15	0.15	0.20	0.20
σ_j^2	0.20	0.10	0.05	0.05	0.10	0.05	0.10	0.15	0.15	0.20
σ_{nugget}^2	0.10									

6 Application: Real Estate Pricing

In prior consultation with real estate experts at Fahrländer Partner, real estate mass appraisal will be done on a model fitted on transactions from six consecutive quarters using (transformed or scaled) covariates given in Table 1. Predictions are then given for the following seventh quarter. The rationale behind this setup is to account for a time trend.

The focus of this application lies – like in previous simulation studies – on two aspects. First, we will compare and analyze the outputs of ML-estimated GP-based models with respect to parameter estimation and interpretation of the estimated SVCs (Section 6.3). Second, we will expand this framework in order to compare the predictive performance of the different methods (Section 6.4). We use a *moving window* validation. That is, we divide the data set into 4 folds ($f = 1, \dots, 4$). Each fold f consists of data from 6 consecutive quarters $\mathcal{S}_{\text{train},f}$ which are used to estimate the model and a following seventh quarter \mathcal{S}_f which is used for evaluating the predictive accuracy. A visualization of the moving windows is given in Table 5.

6.1 SVC Model for Real Estate Pricing

We extend the previous simple model used in Section 2.1 and add *i)* a standardized age $\text{Z.age} = (2000 - \text{yoc})/20$ defined with the year of construction yoc , *ii)* Z.age^2 as one expects a quadratic age effect in hedonic models in Europe (Brunauer et al., 2010; Fahrländer, 2006), *iii)* the renovation rating renov , and *iv)* a dummy variable constructed

Table 5: Moving window validation set up with four folds. The model is fitted on all observations with $s_i \in \mathcal{S}_{\text{train},f}$ and tested out-of-sample on \mathcal{S}_f .

Folds f	2015		2016				2017			
	Q3	Q4	Q1	Q2	Q3	Q4	Q1	Q2	Q3	Q4
1	$\mathcal{S}_{\text{train},1}$						\mathcal{S}_1			
2		$\mathcal{S}_{\text{train},2}$						\mathcal{S}_2		
3			$\mathcal{S}_{\text{train},3}$						\mathcal{S}_3	
4				$\mathcal{S}_{\text{train},4}$						\mathcal{S}_4

from the quarter of transaction. Latter is defined as

$$D_{\text{lastQ}} := \begin{cases} 1, & \text{if transaction took place in the last quarter of the training data,} \\ 0, & \text{otherwise.} \end{cases}$$

This is to differentiate the most recent transactions from the rest of the training set in order to account for the temporal trend and should enhance the predictive performance. In summary, we will obtain the following model with $p = 8$ SVCs:

$$\begin{aligned} y_i := \log \text{price}_i = & \beta_1(s_i) + \beta_2(s_i) \log \text{area}_i + \beta_3(s_i) \text{Z.age}_i \\ & + \beta_4(s_i) \text{Z.age}_i^2 + \beta_5(s_i) \text{micro}_i + \beta_6(s_i) \text{stand}_i \\ & + \beta_7(s_i) \text{renov}_i + \beta_8(s_i) D_{\text{lastQ}} + \varepsilon_i, \end{aligned} \quad (11)$$

where the locations s_i are given in *transformed* LV03 coordinates. More precisely, the easting (LV03x) and northing (LV03y) are now centered on the origin (0;0) and transformed to kilometers, i.e.

$$\begin{pmatrix} \text{Z.LV03x} \\ \text{Z.LV03y} \end{pmatrix} := 10^{-3} \cdot \left(\begin{pmatrix} \text{LV03x} \\ \text{LV03y} \end{pmatrix} - \begin{pmatrix} 600,000 \\ 200,000 \end{pmatrix} \right).$$

This procedure increases numerical stability while still providing interpretability of distances.

6.2 MLE Specifications

The underlying SVC model is (11) where – as in the simulation study – we assume exponential covariance functions for all GPs modeling the SVCs. Further, we use regularization for the ranges and variances, i.e. $\mathbb{P}(\rho_j < 1) = 0.05$ and $\mathbb{P}(\sigma_j > 0.3) = 0.05$ in corresponding units. Due to the large number of observations, we apply covariance tapering. The taper range was set to $\rho^* = 5$ kilometers, as at least half of the observations of the training data have 74 or more neighbors within their taper range, cf. Figure 15 in Appendix B. To stay consistent with the definition in the simulation study, we use the same label MLE.r for this model and above described method specifications.

6.3 Model Output and Interpretation

We start with a single MLE.r model output. It was estimated on $\mathcal{S}_{\text{train},1}$, cf. Table 5. To provide a reference, we compare it to a classical geostatistical model. That is, the underlying model only contains one GP for the intercept, while all other covariates enter

the model only as fixed effects. Though the models differ, we use the same methodology and specification as described for the GP-based SVC model, i.e., profile likelihood optimization using the same regularization and tapering range as previously described. We label it MLE.geo.

The estimated parameters of both the MLE.r and MLE.geo models are given in Table 6. We note that the estimated mean effects are very similar. Moving to the covariance parameters of the SVC model, note that the estimates are indeed very different for ranges and variances. The bias due to covariance tapering is notable in the range parameters $\hat{\rho}_j$. The four range parameters exceeding the taper range ρ^* of 5 kilometers would have an *effective range* of $3\hat{\rho}_j$ with an exponential covariance function. This would translate to effective ranges of – in some cases – well over 200 kilometers, and therefore almost as large as the dimensions of Switzerland. In the context of real estate pricing this would not make sense. But we have to recall that due to tapering all covariance functions are compactly supported on $[0, \rho^*]$.

Table 6: Estimated mean effects, ranges, and variances of the GP-based SVC (MLE.r) and classical geostatistical model (MLE.geo) in the first fold of the moving window validation.

j	SVCs	MLE.r			MLE.geo		
		$\hat{\mu}_j$	$\hat{\rho}_j$	$\hat{\sigma}_j^2$	$\hat{\mu}_j$	$\hat{\rho}_j$	$\hat{\sigma}_j^2$
1	Intercept	8.6448	118.72	0.0210	8.4342	244.70	0.0650
2	log area	0.8796	75.10	0.0010	0.9013	–	–
3	Z.age	–0.1707	4.56	0.0045	–0.1567	–	–
4	Z.age ²	0.0272	3.67	0.0002	0.0317	–	–
5	stand	0.0825	33.64	0.0009	0.0982	–	–
6	micro	0.0820	39.18	0.0012	0.0988	–	–
7	renov	0.0426	1.17	0.0034	0.0494	–	–
8	D_{lastQ}	0.0229	0.72	0.0066	0.0249	–	–
	Nugget	–	–	0.0183	–	–	0.0236

Further, we notice the relatively large estimates for the variance in the intercept as well as the nugget in the SVC model. Although the covariates are not standardized, they do have a similar range of values that they can take, cf. ranges in Table 1. This leads us to believe that, on the one hand, the mean pricing level is one of the dominant factors when it comes to real estate pricing. On the other hand, the large nugget variance suggests that there exists a high residual variability of apartments within the data set.

We will now take a look at the visualized SVCs as in Figure 1, i.e., the intercept, log **area**, and the ratings of micro locations and standard **micro** and **stand**, respectively. These are also the ones with the largest estimated ranges suggesting that the spatial structure will be most prominent in these SVCs. All other covariates SVCs are given in Appendix C.

Recall that due to their definition as zero-mean GPs, the interpretation of ML-estimated SVCs is different than what we saw in Figure 1. For GWR the mean effect of each SVC was included. Therefore, one has to interpret Figure 6 as deviations from mean effects, which are given in Table 6. For the intercept depicted in Figure 6(a), one can clearly see that the mean apartment prices are highest in the agglomerations of Zurich, Geneva, and Basel as well as the alpine resort Saint Moritz. The mean prices are also higher along the shore line of Lake Geneva starting from the city of Geneva and reaching

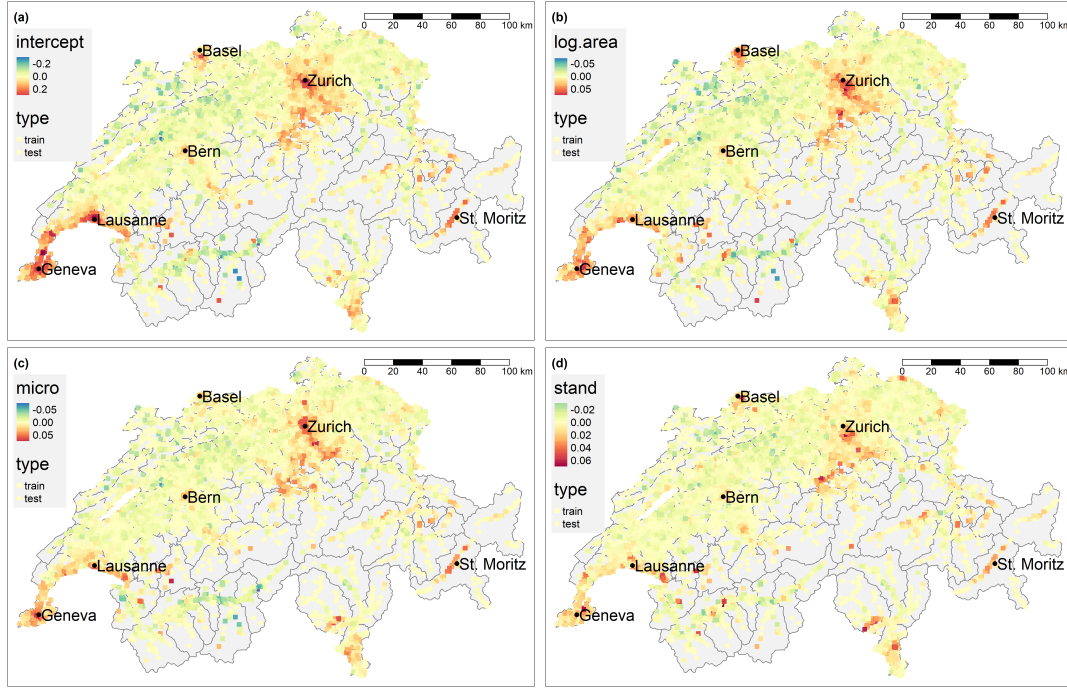


Figure 6: Selection of estimated SVCs of the model (11) using MLE.r as defined in this section. The four facets show SVCs of (a) the intercept, (b) log area, (c) **micro**, and (d) **stand**. The squares indicate training locations $\mathcal{S}_{\text{train},1}$, the dots are extrapolations to all other centroids.

as far as Lausanne. More rural areas such as between Basel and Bern or in the alpine regions south of Bern have lower mean apartment prices. Qualitatively, the overall picture does not change too much when comparing to Figure 6(b) to (d), i.e., the SVCs of log area, **micro**, and **stand**. There are however some differences.

For example, along the shore line of Lake Geneva, the effect of **micro** and **stand** is smaller compared to the city center of Geneva. However, the mean prizes in Lausanne are relatively high. This suggests that the standard or micro location rating of an apartment in Lausanne is not as important as its location.

Overall, the quality of the ML-estimated SVCs as displayed in Figure 6 seems more plausible and in line with expert knowledge compared to GWR-estimated SVCs in Figure 1. There are no highly questionable deviations as seen in Figure 1(a) and (b). Also the estimated ranges vary between the SVCs. For instance, the SVCs for micro location and standard rating are much more locally pronounced as compared to the intercept and log area. Such properties cannot be modeled by GWR.

6.4 Predictive Performance

In this last part of the real estate application, we evaluate the predictive performance of MLE.r, MLE.geo, GWR and ESF. The SPDE method cannot be considered as there are too many hyper parameters for INLA. In order to compare the predictive performance of the different approaches, we use the moving window validation setting introduced in Table 5. For each fold $f \in \{1, 2, 3, 4\}$ and method $m \in \{\text{MLE.r, MLE.geo, GWR, ESF}\}$, we fit a model $g(\cdot; m, f)$ on the data $\mathcal{S}_{\text{train},f}$ and then make predictions for out-of-sample observations $\iota \in \mathcal{S}_f$. Thus, we have $\hat{y}_\iota^{(m,f)} := g(\mathbf{x}_\iota; m, f)$. By doing so, we can compute

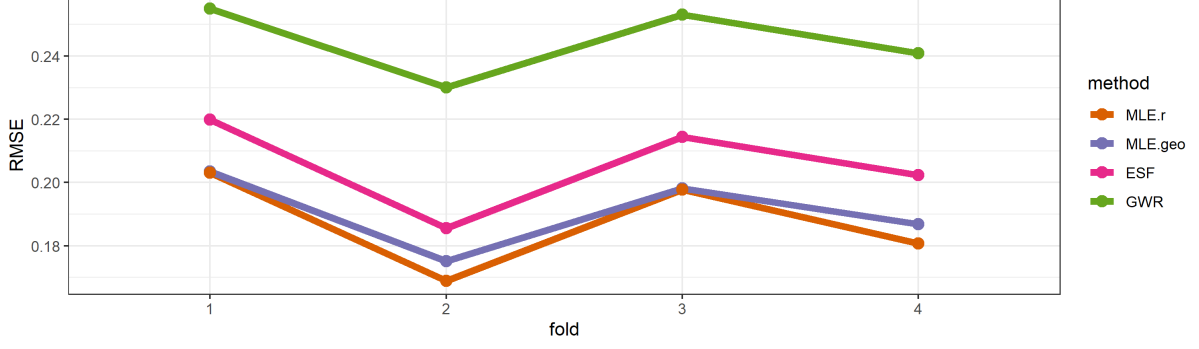


Figure 7: $\text{RMSE}_f^{(m)}$ as defined in (13) of the moving window validation.

the prediction errors and the RMSE as follows:

$$e_t^{(m)} := y_t - \hat{y}_t^{(m,f)} \quad (12)$$

$$\text{RMSE}_f^{(m)} := \sqrt{\frac{1}{|\mathcal{S}_f|} \sum_{t \in \mathcal{S}_f} \left(e_t^{(m)} \right)^2} \quad (13)$$

We depict the results for the RMSE in Figure 7. We find that the GP-based SVC model performs best. Further, it shows that model-based methods outperform ESF and especially GWR throughout all folds. The differences between both MLE for an SVC and a geostatistical model are relatively small.

In the following, we investigate whether the differences are significant by using a mixed effect model describing the RMSE as defined in (13). The reference method is the MLE-based SVC model MLE.r defined as the intercept α_0 . For the methods MLE.geo, ESF, and GWR we include deviations α_m from the reference level α_0 . Further, we include a random effect for the fold, i.e. a temporal effect, with iid $\zeta_f \sim \mathcal{N}(0, \sigma_t^2)$ as well as an iid noise variable $\varepsilon_{f,m} \sim \mathcal{N}(0, \sigma^2)$. The model describing the RMSE is therefore given by

$$\text{RMSE}_f^{(m)} = \alpha_0 + \alpha_m + \zeta_f + \varepsilon_{f,m}. \quad (14)$$

The model has been estimated using the R package `lmerTest` (Kuznetsova et al., 2017) and the main results are given in Table 7, while the whole analysis can be found in the supplementary material. They confirm the conclusions drawn from Figure 7. In particular, the RMSE for ESF and GWR are significantly higher than for MLE methods. However, the difference in RMSE between MLE.r and MLE.geo is not significant at 5% level.

6.4.1 Detailed Prediction Error Analysis

In the following, we perform a detailed prediction error analysis that takes into account that errors of the different methods for the same apartments are correlated. Similarly to model (14), we analyze the prediction errors as defined in (12) using a mixed effect model. The independent variables contain a fixed effect for each method which we define with γ_m . Further, notice that we have repeated measures, since every apartment has been predicted by each method. We can account for this by an iid random effect $\zeta_t \sim \mathcal{N}(0, \sigma_{\text{ap}}^2)$ for the different apartments. Finally, we add iid $\varepsilon_{t,m} \sim \mathcal{N}(0, \sigma_m^2)$ for the noise with distinct standard deviation for each method. The underlying mixed effect model is

$$e_t^{(m)} = \gamma_m + \zeta_t + \varepsilon_{t,m}. \quad (15)$$

When estimating the model, we expect the estimates of γ_m to be near 0, since the predictions should be unbiased. Further, the main focus should be on the estimated standard deviations σ_m of the noise, as they indicate the uncertainty of the corresponding methods. The estimation was conducted using the R package `nlme` (Pinheiro et al., 2018) and the main results are given in Table 7. The estimated fixed effects are in fact close to 0, the estimated standard deviations are increasing throughout the methods indicating a higher precision for predictions under MLE. The standard deviation for the apartment-specific random effect was estimated with $\hat{\sigma}_{\text{ap}} = 0.1821$. This again indicates the high variability of apartments that the models have to predict. The full analysis can be found in the supplementary material.

Table 7: Estimated parameters of the RMSE model (14) and error model (15). The estimated coefficients are given with their corresponding standard errors in paranthesis. Note that in the RMSE model the reference level is the MLE.r method ($\hat{\alpha}_0 = 0.1877$). Further, the p -values for two-sided t -tests of $H_0: \alpha_m = 0$ and the estimated standard deviations $\hat{\sigma}_m$ of model (15) are given.

Methods m	Model (14)		Model (15)	
	$\hat{\alpha}_m$	p -value	$\hat{\gamma}_m$	$\hat{\sigma}_m$
MLE.r	—	—	−0.0037 (0.0018)	0.0451
MLE.geo	0.0032 (0.0016)	0.0751	−0.0014 (0.0018)	0.0535
ESF	0.0179 (0.0016)	0.0000	0.0045 (0.0021)	0.1195
GWR	0.0571 (0.0016)	0.0000	−0.0074 (0.0024)	0.1755

6.4.2 Probabilistic Predictions

The GP-based geostatistical and SVC model allow us to provide a predictive distribution instead of merely a point prediction. We use the *continuous ranked probability score* (CRPS) proposed by Gneiting and Raftery (2007) to assess the accuracy of the predictive distributions. The results are depicted in Figure 8. Compared to Figure 7 with the RMSE, one can observe that the SVC model has an advantage with respect to quantifying the uncertainty over the geostatistical model with only having spatially varying intercept.

6.4.3 Summary Predictive Performance

The extensive investigation of predictive performance in the real estate application showed that the MLE method applied on the GP-based models performs considerably better than the other methods, while offering the possibility to quantify the uncertainty of predictions. When it comes to the comparison of the geostatistical to the SVC model, the differences are more subtle. In our application, the gain by modeling and predicting the apartment prices with SVC models instead of geostatistical models is small, whereas the SVC model quantifies uncertainties better. As mentioned in Section 6.3, this might be due to the location as a dominant factor in real estate mass appraisal.

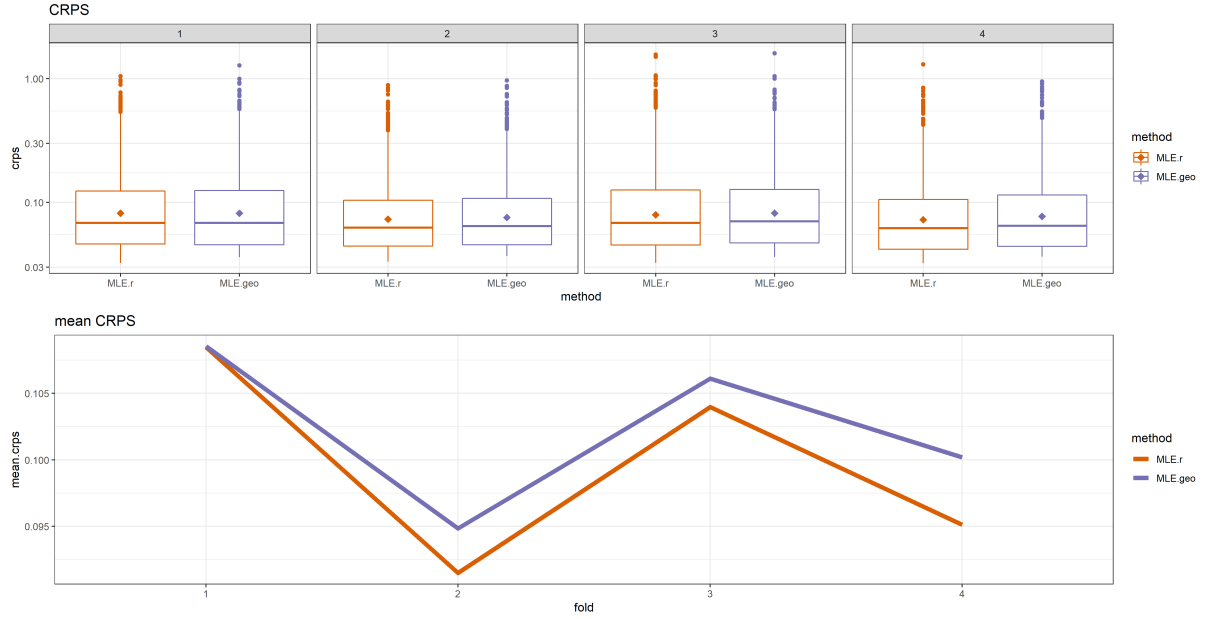


Figure 8: Specific (upper box plots) and mean (lower line plot) CRPS of the MLE methods for the geostatistical model (MLE.geo) and the SVC model (MLE.r) in each fold. Note that the y -axis in the upper panel is log-scaled. The values have been computed using the R package `scoringRules` (Jordan et al., 2019).

7 Conclusion

In this paper, we presented an MLE approach for GP-based SVC models. We empirically validated our approach against other, existing methods for SVC models. This has been done in a simulation study as well as an application with real estate data. To the best of our knowledge, our proposed methodology is the only implemented and currently available method to estimate and make predictions for GP-based SVC models in context of large data where both the sample size and the number of SVC is large.

Parameter estimations were shown to be accurate and unbiased when not applying covariance tapering. The predictive performance is in both the simulation study as well as the application among the best. In contrast to not model based approaches such as GWR and ESF it is able to quantify uncertainty by giving predictive variance.

All GPs were defined by exponential covariance functions and based on Euclidean distances in a two-dimensional domain. However, our proposed method can easily be extended to allow GP-based SVC models defined by individual, non-stationary (anisotropic) covariance functions using other norms on higher dimensional domains $D \subset \mathbb{R}^d$ with $d \geq 3$. Here, MLE could even be augmented to estimate, say, the smoothness.

We make some final remarks on future work: First and foremost, it would be greatly appreciated to see further comparisons of existing SVC methods on other data sets to see how the predictive performance compares.

Further, multicollinearity issues with GWR have been raised by Wheeler and Tiefelsdorf (2005) and one should also investigate if this translates to our methodology. This is in accordance with some SVC selection method that has to be developed to check whether a coefficient is constant or spatially varying.

Acknowledgment

We gratefully acknowledge the support by the Swiss Innovation Agency *Innosuisse*, project number 28408.1 PFES-ES. We would like to thank Leonhard Held for his helpful comments on this paper. We also would like to thank Manuel Lehner and Jaron Schlesinger from Fahrländer Partner for their valuable input towards the application with real estate appraisal.

Supplementary Material

The code for computation is available online under <https://git.math.uzh.ch/jdambo/open-access-svc-paper>. Additionally, we provide the following supplementary material.

Appendix: Additional results and figures. (PDF)

R package varycoef: R package by Dambo et al. (2019) containing the routines of the MLE method for SVC models described in this article. (GNU zipped tar file)

Bibliography

- Bakar, K. S., P. Kokic, and H. Jin (2016). Hierarchical Spatially Varying Coefficient and Temporal Dynamic Process Models Using **spTDyn**. *Journal of Statistical Computation and Simulation* 86(4), 820–840.
- Banerjee, S., A. E. Gelfand, A. O. Finley, and H. Sang (2008). Gaussian Predictive Process Models for Large Spatial Data Sets. *Journal of the Royal Statistical Society: Series B (Statistical Methodology)* 70(4), 825–848.
- Bivand, R. and D. Yu (2017). **spgwr**: Geographically Weighted Regression. R Package Version 0.6-32, <https://CRAN.R-project.org/package=spgwr>.
- Brunauer, W. A., S. Lang, P. Wechselberger, and S. Bienert (2010). Additive Hedonic Regression Models with Spatial Scaling Factors: An Application for Rents in Vienna. *The Journal of Real Estate Finance and Economics* 41(4), 390–411.
- Byrd, R. H., P. Lu, J. Nocedal, and C. Zhu (1995). A Limited Memory Algorithm for Bound Constrained Optimization. *SIAM Journal on Scientific Computing* 16(5), 1190–1208.
- Cao, K., M. Diao, and B. Wu (2019). A Big DataBased Geographically Weighted Regression Model for Public Housing Prices: A Case Study in Singapore. *Annals of the American Association of Geographers* 109(1), 173–186.
- Cressie, N. (1990). The Origins of Kriging. *Mathematical Geology* 22(3), 239–252.
- Cressie, N. (2011). *Statistics for Spatio-Temporal Data*. Wiley Series in Probability and Statistics. Hoboken, N.J: Wiley.
- Dambo, J. A., F. Sigrist, and R. Furrer (2019). **varycoef**: Varying Coefficients. R Package Version 0.2.9, <https://cran.r-project.org/package=varycoef>.

- Dray, S., P. Legendre, and P. R. Peres-Neto (2006). Spatial Modelling: A Comprehensive Framework for Principal Coordinate Analysis of Neighbour Matrices (PCNM). *Ecological Modelling* 196(3), 483 – 493.
- Environmental Systems Research Institute (ESRI) (2020). ArcGIS Pro. <http://pro.arcgis.com/en/pro-app/tool-reference/spatial-statistics/geographicallyweightedregression.htm>.
- Fahrlander, S. S. (2006). Semiparametric Construction of Spatial Generalized Hedonic Models for Private Properties. *Swiss Journal of Economics and Statistics* 142(4), 501–528.
- Federal Office of Topography *swisstopo* (1900). LV03. <https://www.swisstopo.admin.ch/en/knowledge-facts/surveying-geodesy/reference-frames/local/lv03.html>.
- Finley, A. O. (2010). Comparing Spatially-Varying Coefficients Models for Analysis of Ecological Data with Non-Stationary and Anisotropic Residual Dependence. *Methods in Ecology and Evolution* 2(2), 143–154.
- Fotheringham, A. S., C. Brunsdon, and M. Charlton (2002). *Geographically Weighted Regression: The Analysis of Spatially Varying Relationships*. Chichester: Wiley.
- Franco-Villoria, M., M. Ventrucchi, and H. Rue (2019). A Unified View on Bayesian Varying Coefficient Models. *Electronic Journal of Statistics* 13(2), 5334–5359.
- Fuglstad, G.-A., D. P. Simpson, F. K. Lindgren, and H. Rue (2018). Constructing Priors that Penalize the Complexity of Gaussian Random Fields. *Journal of the American Statistical Association* 114(525), 445–452.
- Furrer, R., F. Bachoc, and J. Du (2016). Asymptotic Properties of Multivariate Tapering for Estimation and Prediction. *Journal of Multivariate Analysis* 149, 177–191.
- Furrer, R., M. G. Genton, and D. W. Nychka (2006). Covariance Tapering for Interpolation of Large Spatial Datasets. *Journal of Computational and Graphical Statistics* 15(3), 502–523.
- Gelfand, A. E., H.-J. Kim, C. F. Sirmans, and S. Banerjee (2003). Spatial Modeling with Spatially Varying Coefficient Processes. *Journal of the American Statistical Association* 98(462), 387–396.
- Geng, J., K. Cao, L. Yu, and Y. Tang (2011). Geographically Weighted Regression Model (GWR) based Spatial Analysis of House Price in Shenzhen. In *2011 19th International Conference on Geoinformatics*, pp. 1–5.
- Gneiting, T. and A. E. Raftery (2007). Strictly Proper Scoring Rules, Prediction, and Estimation. *Journal of the American Statistical Association* 102(477), 359–378.
- Griffith, D. A. (2011). *Spatial Autocorrelation and Spatial Filtering: Gaining Understanding through Theory and Scientific Visualization*. Advances in Spatial Science. Berlin: Springer.

- Heaton, M. J., A. Datta, A. O. Finley, R. Furrer, J. Guinness, R. Guhaniyogi, F. Gerber, R. B. Gramacy, D. Hammerling, M. Katzfuss, F. K. Lindgren, D. W. Nychka, F. Sun, and A. Zammit-Mangion (2019). A Case Study Competition Among Methods for Analyzing Large Spatial Data. *Journal of Agricultural, Biological and Environmental Statistics* 24(3), 398–425.
- Jordan, A., F. Krüger, and S. Lerch (2019). Evaluating Probabilistic Forecasts with `scoringRules`. *Journal of Statistical Software* 90(12), 1–37.
- Kuznetsova, A., P. B. Brockhoff, and R. H. B. Christensen (2017). `lmerTest` Package: Tests in Linear Mixed Effects Models. *Journal of Statistical Software* 82(13), 1–26.
- Li, F. and H. Sang (2019). Spatial Homogeneity Pursuit of Regression Coefficients for Large Datasets. *Journal of the American Statistical Association* 114(527), 1050–1062.
- Lindgren, F. K. and H. Rue (2015). Bayesian Spatial Modelling with R-INLA. *Journal of Statistical Software, Articles* 63(19), 1–25.
- Lindgren, F. K., H. Rue, and J. Lindström (2011). An Explicit Link between Gaussian Fields and Gaussian Markov Random Fields: The Stochastic Partial Differential Equation Approach. *Journal of the Royal Statistical Society: Series B (Statistical Methodology)* 73(4), 423–498.
- Malpezzi, S. (2008). *Hedonic Pricing Models: A Selective and Applied Review*, Chapter 5, pp. 67–89. John Wiley & Sons, Ltd.
- Murakami, D. (2018). `spmoran`: Moran’s Eigenvector-Based Spatial Regression Models. R package version 0.1.5, <https://CRAN.R-project.org/package=spmoran>.
- Murakami, D. and D. A. Griffith (2015). Random Effects Specifications in Eigenvector Spatial Filtering: A Simulation Study. *Journal of Geographical Systems* 17(4), 311–331.
- Pinheiro, J. C., D. M. Bates, S. DebRoy, D. Sarkar, and R Core Team (2018). `nlme`: Linear and Nonlinear Mixed Effects Models. R package version 3.1-137, <https://CRAN.R-project.org/package=nlme>.
- Rue, H. and L. Held (2005). *Gaussian Markov Random Fields: Theory And Applications (Monographs on Statistics and Applied Probability)*. Chapman & Hall/CRC.
- Rue, H., S. Martino, and N. Chopin (2009). Approximate Bayesian Inference for Latent Gaussian Models by using Integrated Nested Laplace Approximations. *Journal of the Royal Statistical Society: Series B (Statistical Methodology)* 71(2), 319–392.
- Rue, H., A. Riebler, S. H. Sørbye, J. B. Illian, D. P. Simpson, and F. K. Lindgren (2017). Bayesian Computing with INLA: A Review. *Annual Review of Statistics and Its Application* 4(1), 395–421.
- Simpson, D. P., H. Rue, A. Riebler, T. G. Martins, and S. H. Sørbye (2017). Penalising Model Component Complexity: A Principled, Practical Approach to Constructing Priors. *Statistical Science* 32(1), 1–28.

- Stein, M. L. (1999). *Interpolation of Spatial Data: Some Theory for Kriging*. Springer Series in Statistics. New York, NY: Springer New York.
- van Eggermond, M., M. Lehner, and A. Erath (2011). Modeling Hedonic Prices in Singapore. https://www.researchgate.net/publication/266868391_MODELING_HEDONIC_PRICES_IN_SINGAPORE.
- Wheeler, D. C., A. Páez, J. Spinney, and L. A. Waller (2014). A Bayesian Approach to Hedonic Price Analysis. *Papers in Regional Science* 93(3), 663–683.
- Wheeler, D. C. and M. Tiefelsdorf (2005). Multicollinearity and Correlation among Local Regression Coefficients in Geographically Weighted Regression. *Journal of Geographical Systems* 7(2), 161–187.
- Wheeler, D. C. and L. A. Waller (2009). Comparing Spatially Varying Coefficient Models: A Case Study Examining Violent Crime Rates and their Relationships to Alcohol Outlets and Illegal Drug Arrests. *Journal of Geographical Systems* 11(1), 1–22.

Appendix to:
Maximum Likelihood Estimation of Spatially Varying
Coefficient Models for Large Data with an Application to Real
Estate Price Prediction

A Further Results: Simulation Studies

In this section, we show all the results of the simulation study that were only mentioned or not shown at all in the main article.

A.1 Simulation 1: Base Setup

The following show the results as in Figure 4 for Simulation 1 but with GWR included, cf. Figure 9. As one can see, the RMSE of GWR particularly for the intercept is far off. This translates further to bad predictions for the response.

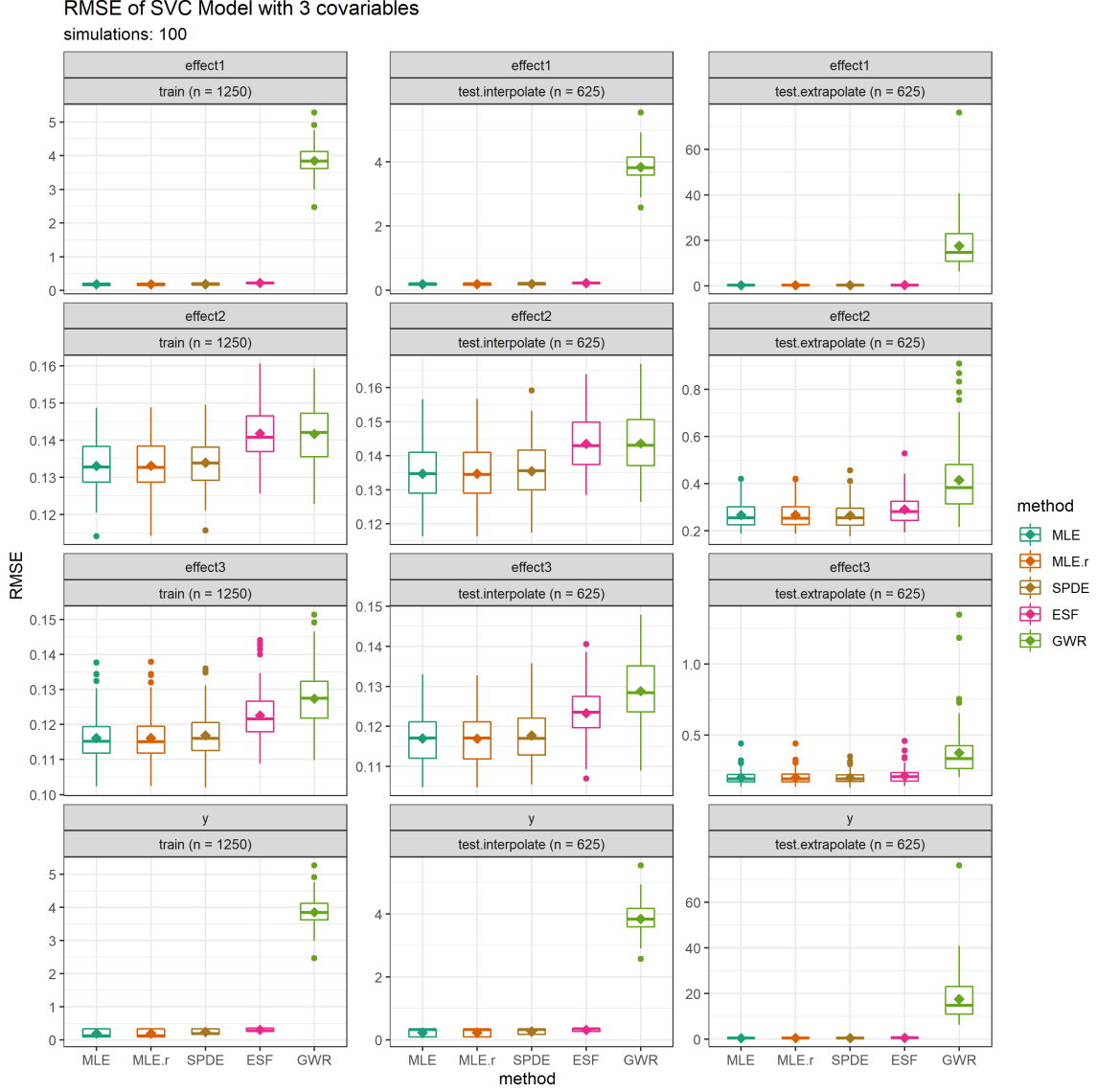


Figure 9: Box plots of RMSE for Simulation 1 as given in Figure 4, but with GWR. The diamonds indicate the means.

A.2 Simulation 2: Number of Observations is $n' = 10,000$

As Figures 4 and 9 for Simulation 1, we give the RMSE for Simulation 2 in the following. The first figure does not include GWR for better readability sake, the second figure includes GWR for completeness sake.

In Figure 10, the calculated RMSE shows that while applying covariance tapering MLE is at least as good as ESF. The MLE methods perform similarly to SPDE, yet they are surpassed by SPDE in SVCs 2 and 3 for within the training and interpolation sets.

In Figure 11, we see that GWR struggles modeling the intercept as in Simulation 1. Additionally, the performance on the extrapolation set produces bad results, too. This confirms the suggestion to use GWR as an explorative tool only. We further show all estimated parameters of Simulation 2 in Figure 12. Here we clearly see improbable results for the estimated ranges using MLE as the only method without regularization.

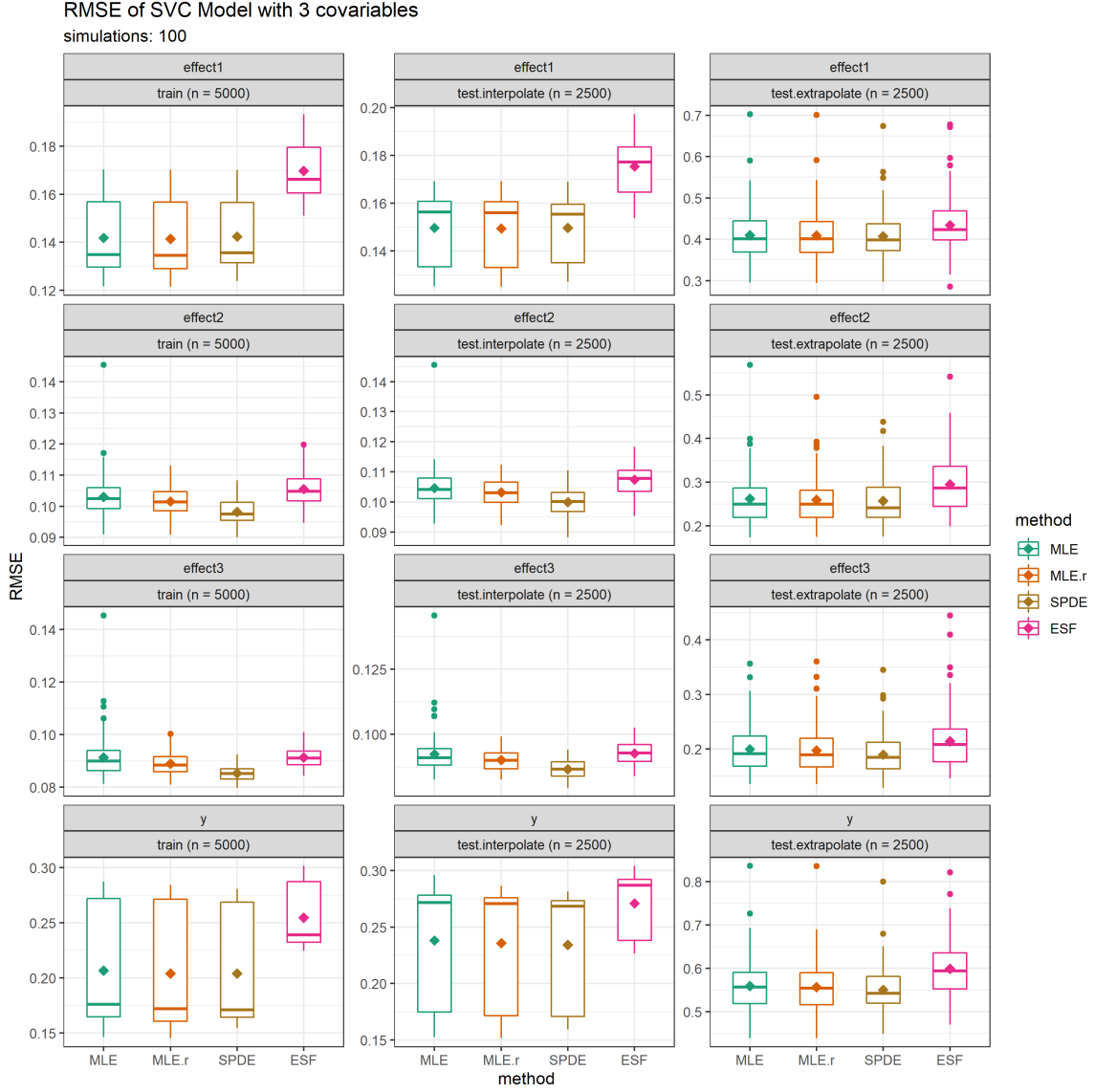


Figure 10: Box plots of RMSE between true β_j and $\hat{\beta}_j$ as well as between \mathbf{y} and $\hat{\mathbf{y}}$ for Simulation 2 in corresponding partition, see (9) and (10). GWR is not given due to better readability. The diamonds indicate the means. Note the different ranges of the y -axis.

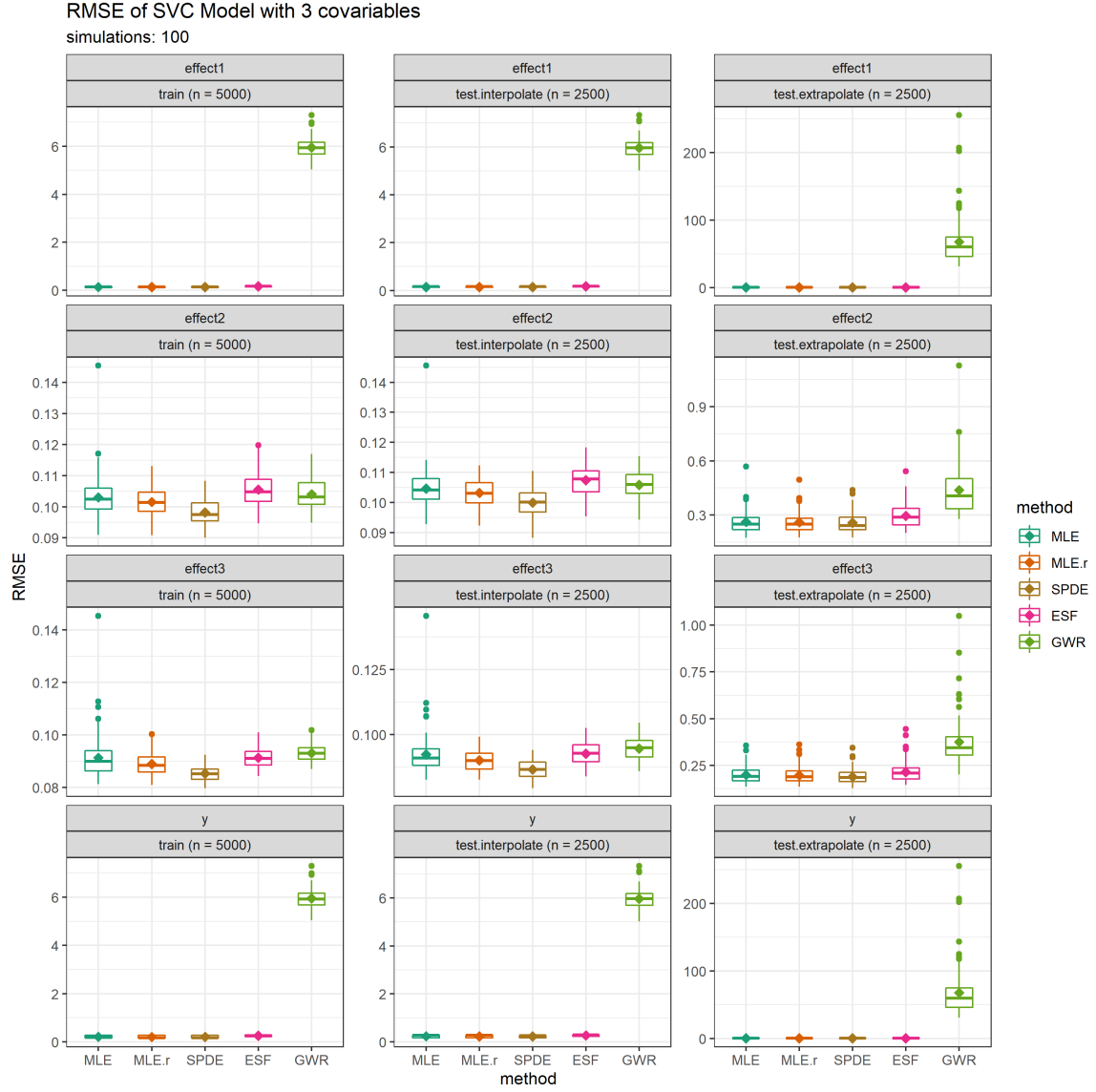


Figure 11: Box plots of RMSE for Simulation 2 including GWR. The diamonds indicate the means. Note the different ranges of the y -axis.

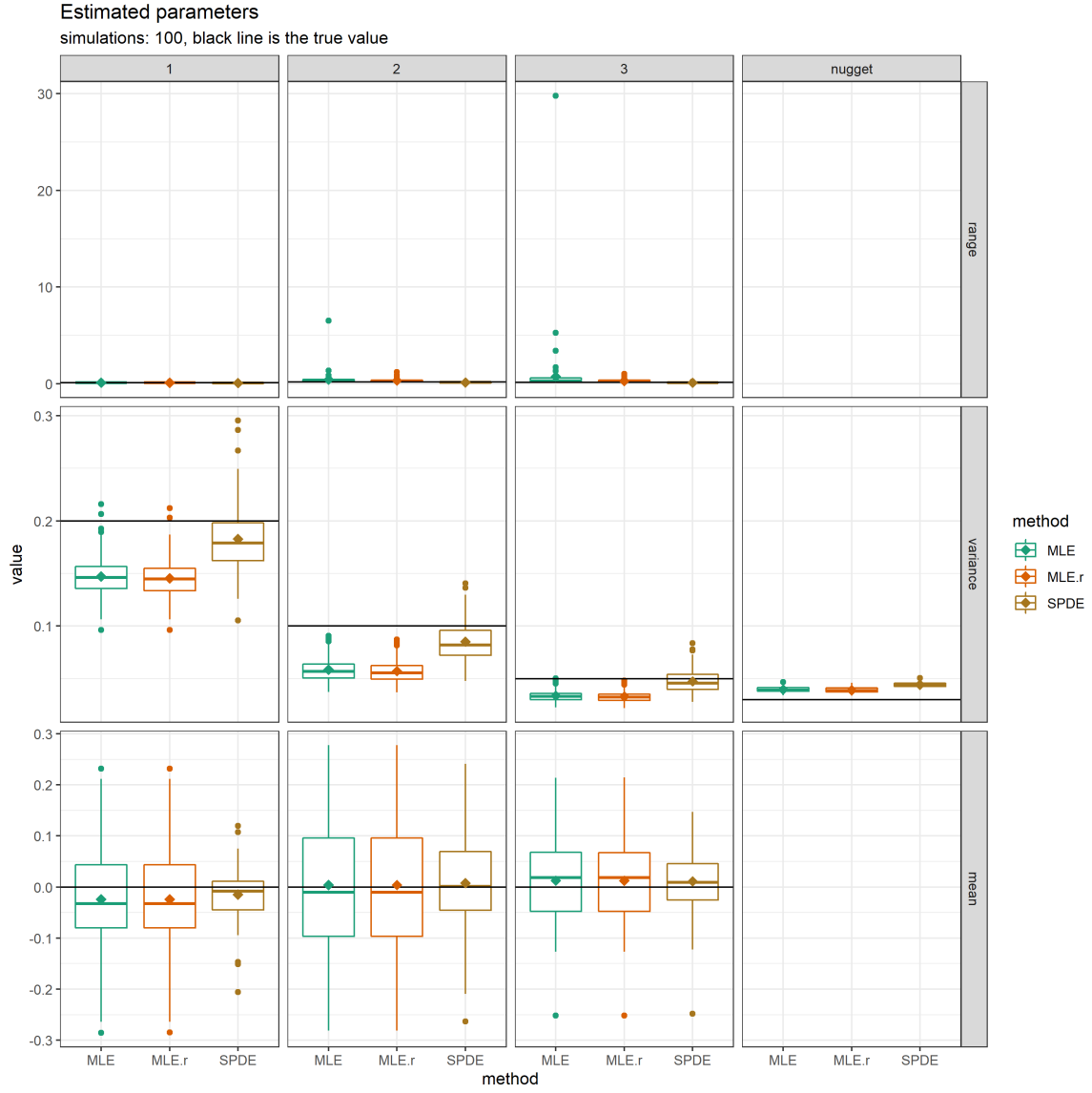


Figure 12: Estimated covariance and mean parameters of all methods of the 100 simulations given as box plots in Simulation 2. The diamonds indicate the means. True values are given by black lines.

A.3 Simulation 3: Number of SVC is $p = 10$

In this simulation, MLE is the only method to estimate the parameters of the SVC model. The accuracy in doing so is surprisingly good. The mean parameters were all estimated without bias and with a deviation proportional to the corresponding variance of the respective GP. The ranges of most SVC are slightly biased in the sense that they are underestimated. This probably leads to underestimated variances, too.

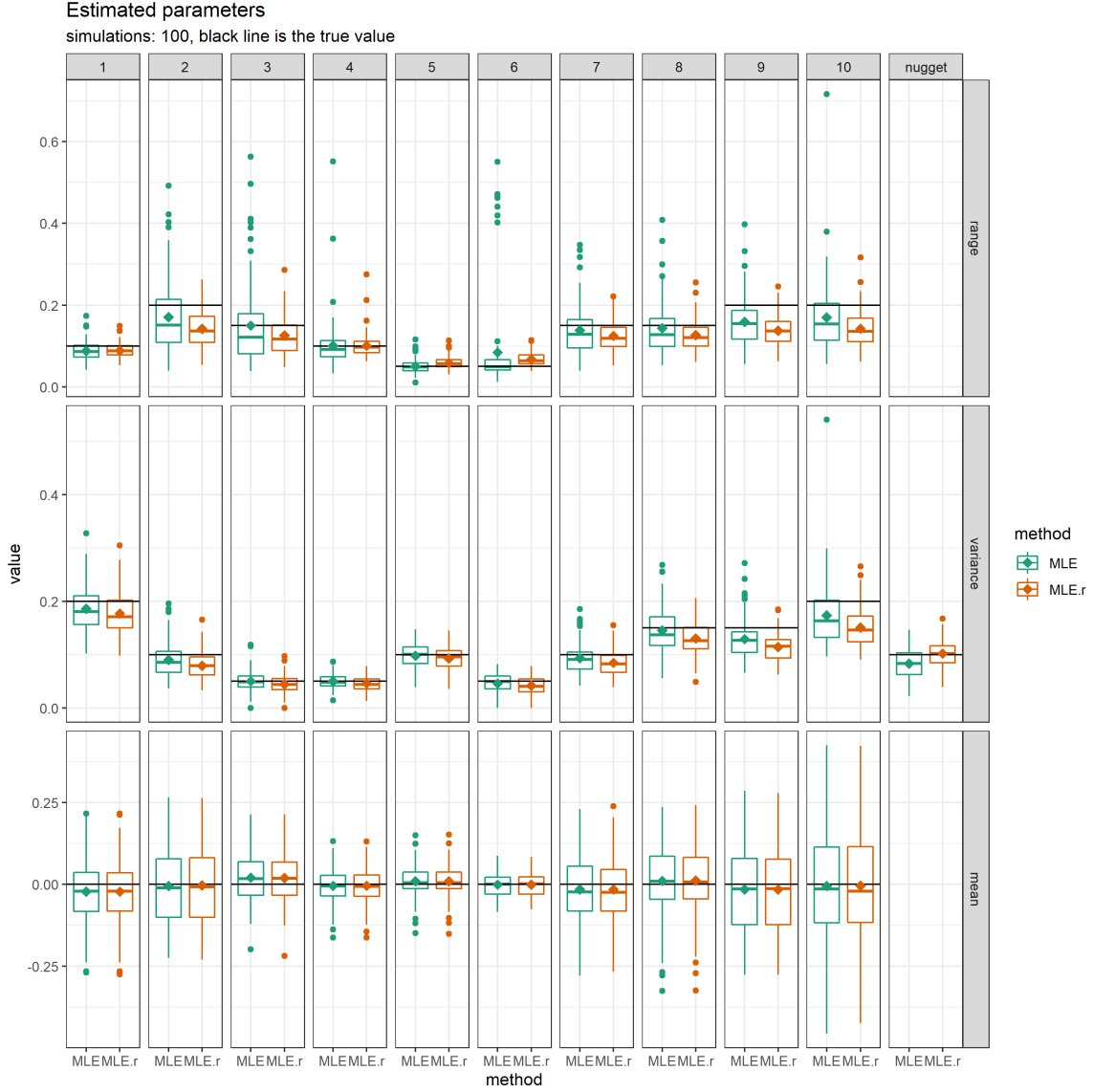
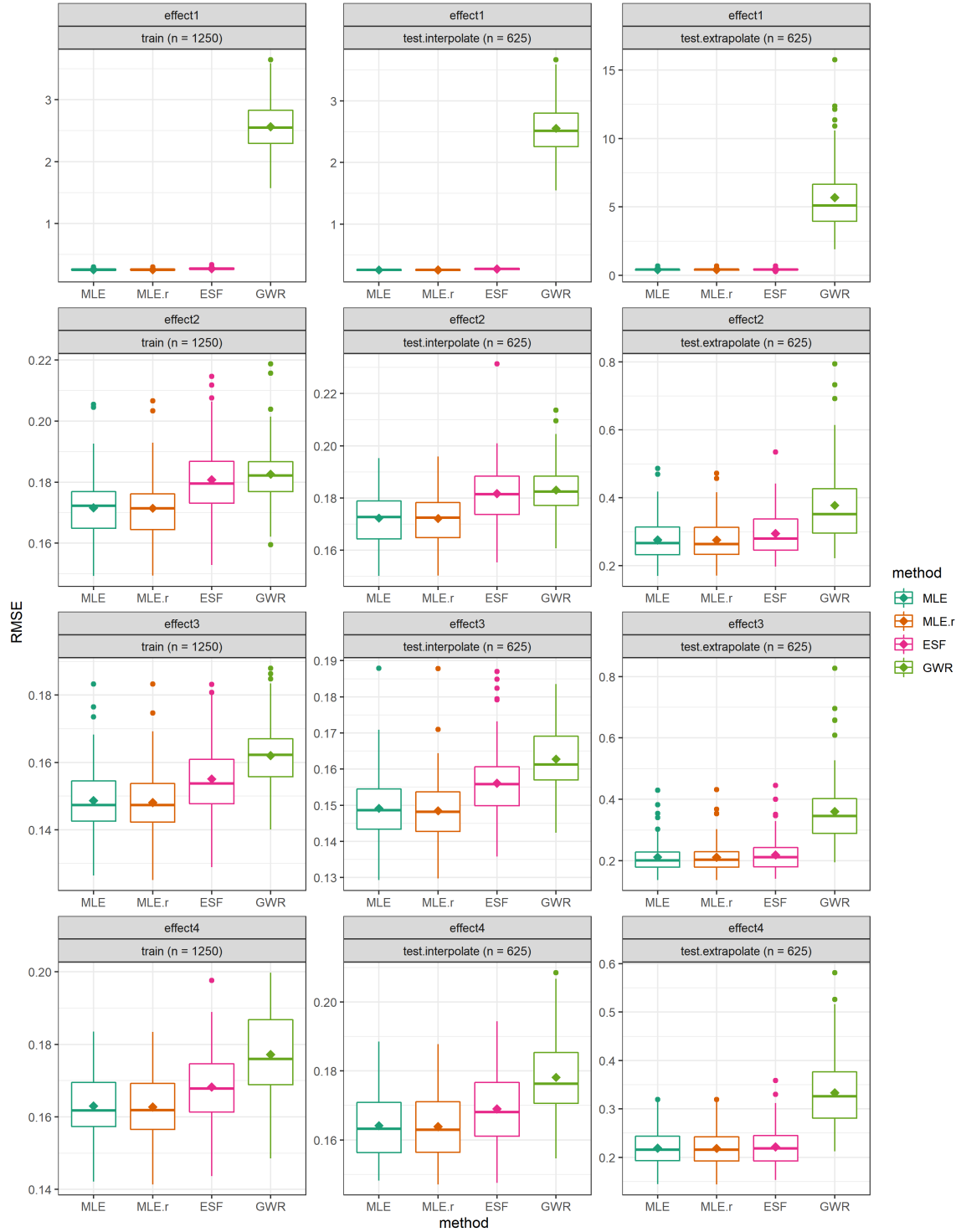


Figure 13: Box plots of RMSE for Simulation 3 without GWR. The diamonds indicate the means.

Over the next 3 pages we show the RMSE for Simulation 3.

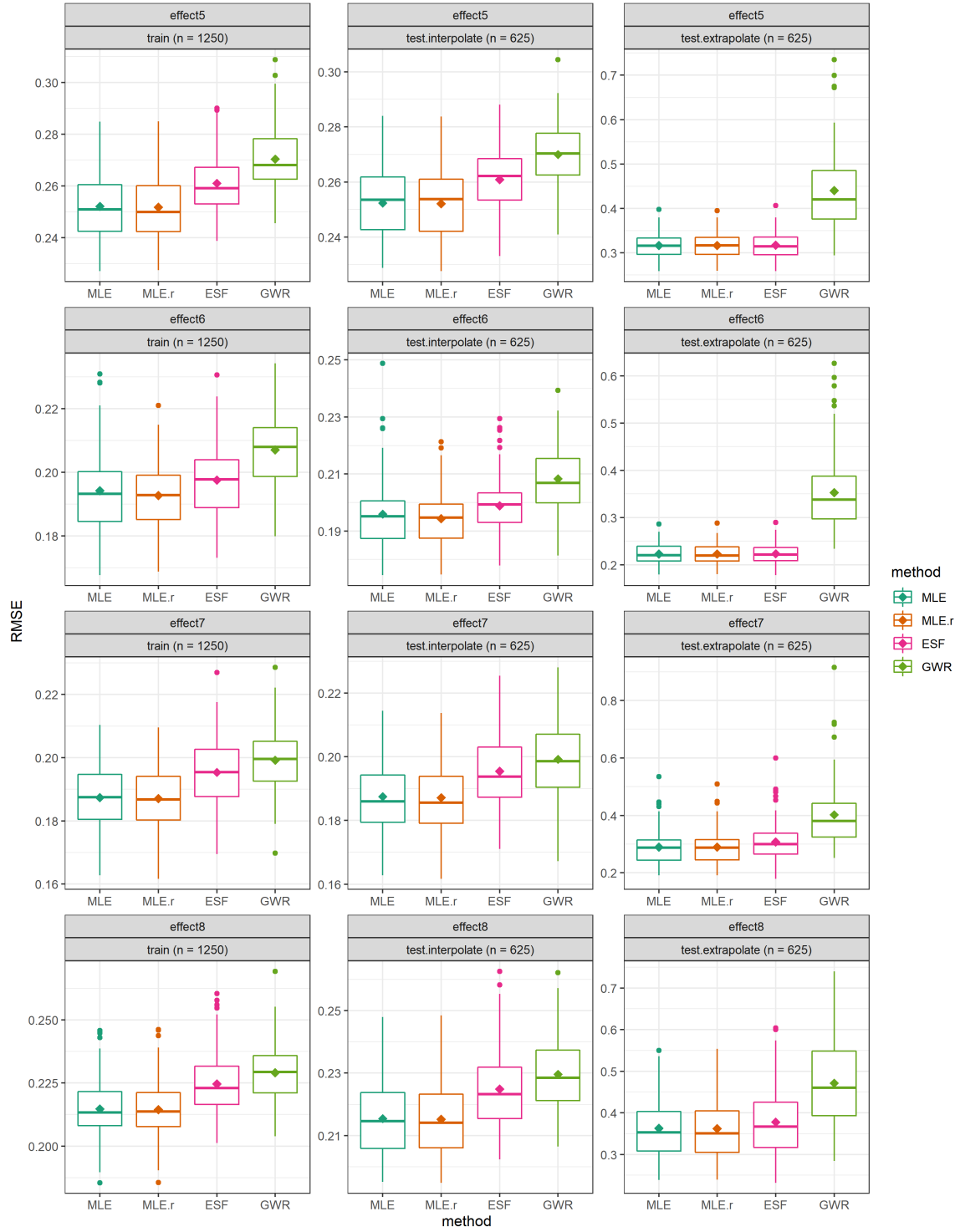
RMSE of SVC Model with 10 covariables

simulations: 100



RMSE of SVC Model with 10 covariables

simulations: 100



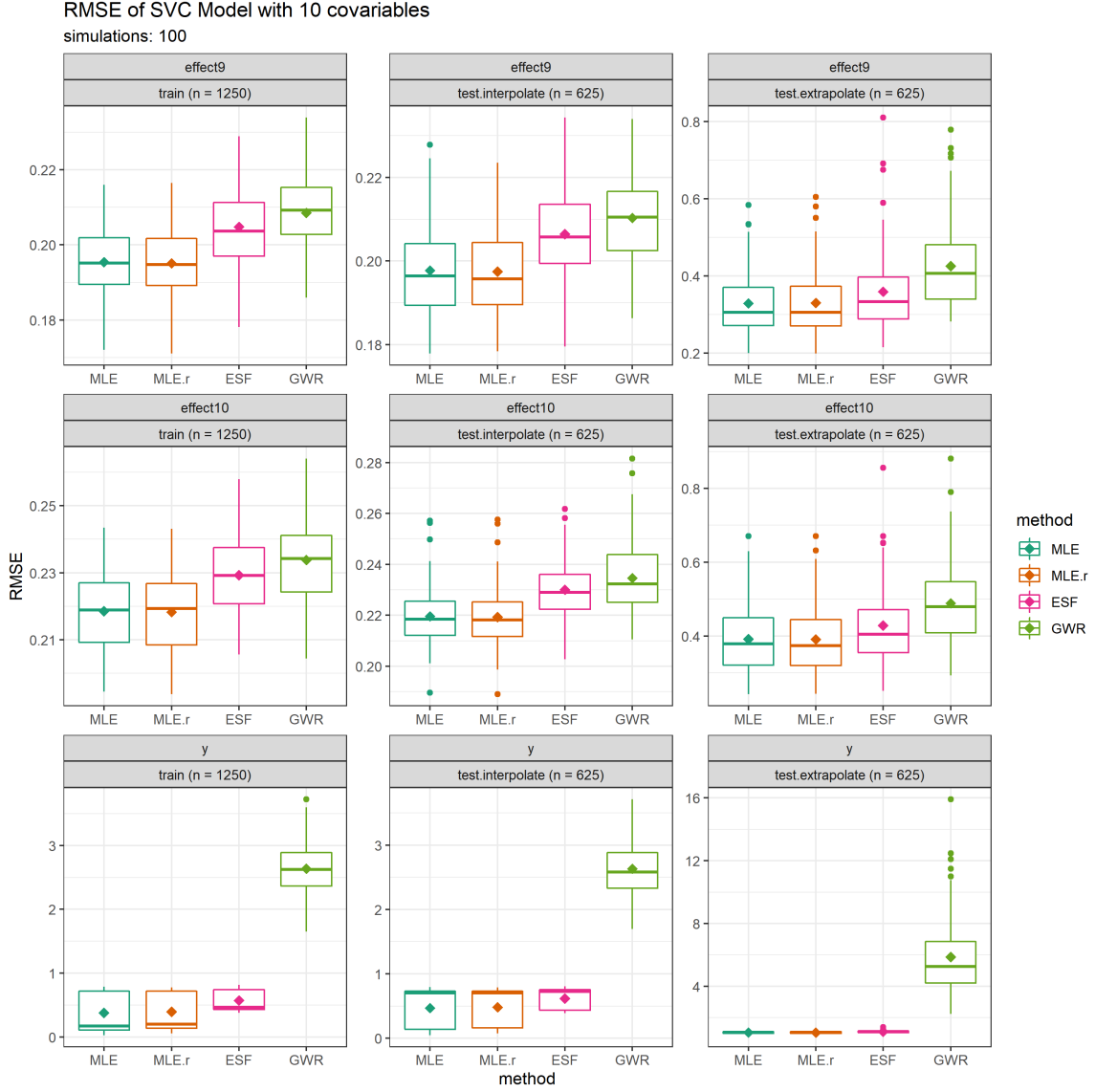


Figure 14: Box plots of RMSE between true β_j and $\hat{\beta}_j$ as well as between \mathbf{y} and $\hat{\mathbf{y}}$ for Simulation 3 in corresponding partition, see (9) and (10). The diamonds indicate the means. Note the different ranges of the y -axis.

B Choice of Taper Range

In order to make a good choice on the taper range for MLE.geo and MLE.r, we have to investigate how many neighbors each observation with a given taper range has. Thus, we compute the *number of neighbors* for an observation i as

$$nn_i^{\rho^*} := \sum_{j \neq i} 1_{\{\|s_i - s_j\| \leq \rho^*\}},$$

where 1_A is the indicator function which is 1 if A holds true and 0 otherwise. We computed $nn_i^{\rho^*}$ for two taper ranges $\rho^* \in \{5, 10\}$. The density and some summary statistics are depicted in Figure 15 for each fold. The median of $nn_i^{\rho^*=5}$ is at least 74 over all folds and the first quartile is at least 38 over all folds, respectively. The maximum does not exceed 575, meaning that there is no observation with more than 575 neighbors within a radius of 5 kilometers. In the case of $\rho^* = 10$ we see that the maximum of $nn_i^{\rho^*=10}$ exceeds 1000 in all folds, which is why we choose a 5 kilometer range over a 10 kilometer range.

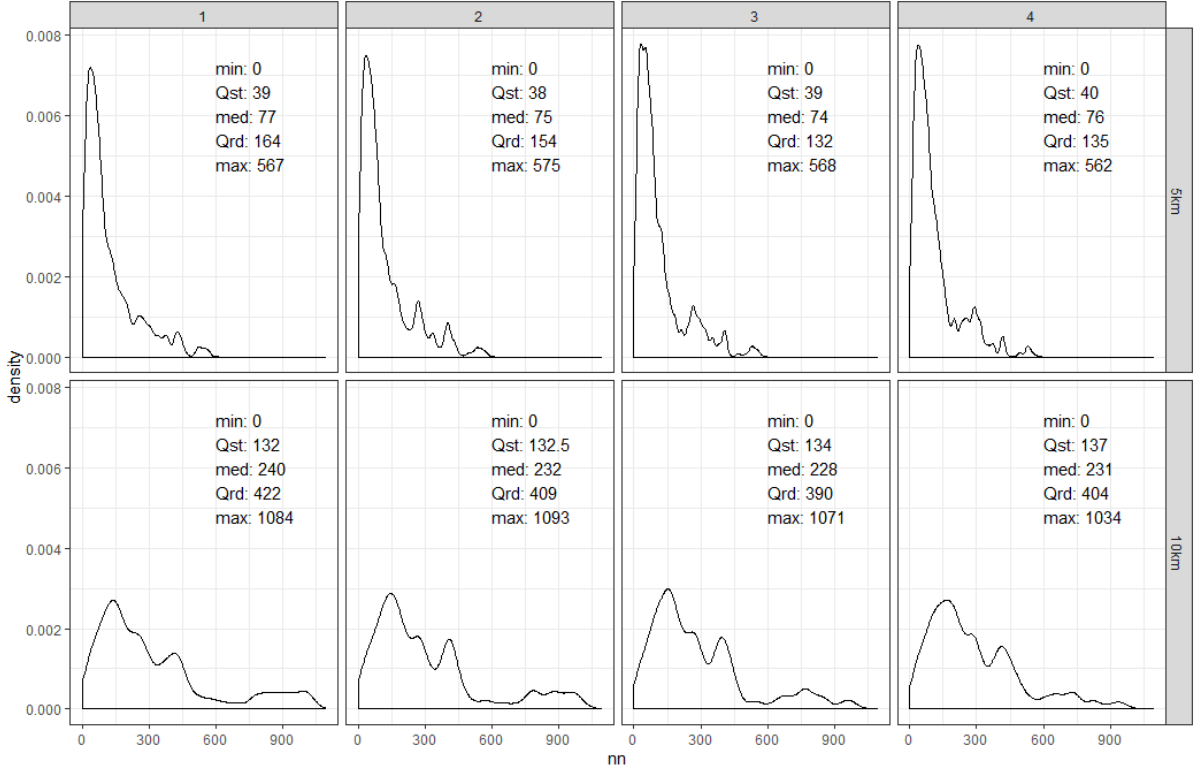


Figure 15: The densities of $nn_i^{\rho^*}$ for $\rho^* \in \{5, 10\}$ and each fold are given in corresponding facets. Additionally, we give the respective quartiles.

C Estimated SVC

Finally, we show the other estimated SVC for fold $f = 1$, as we did in Figure 6 for the MLE.r method. These are the deviations $\hat{\eta}_j$ from the corresponding mean μ_j , which added result in a single SVC for a covariate.

Age: Of the four SVC yet not discussed in this paper, both the linear as well as quadratic effect of the age covariate have the most pronounced spatial structure, cf. Figure 16(a) and (b). One can see that the effect of age in agglomerations is very different from more rural areas. This is consistent with the assumption that – marginally – in rural areas one expects pure depreciation of an apartment with increasing age, while within city centers newly built and old (apartments with year of construction prior to 1920) are higher priced.

Renovation Rating and Last Quarter: Both of these covariates do not have very strong spatial structures, cf. Figure 16(c) and (d).

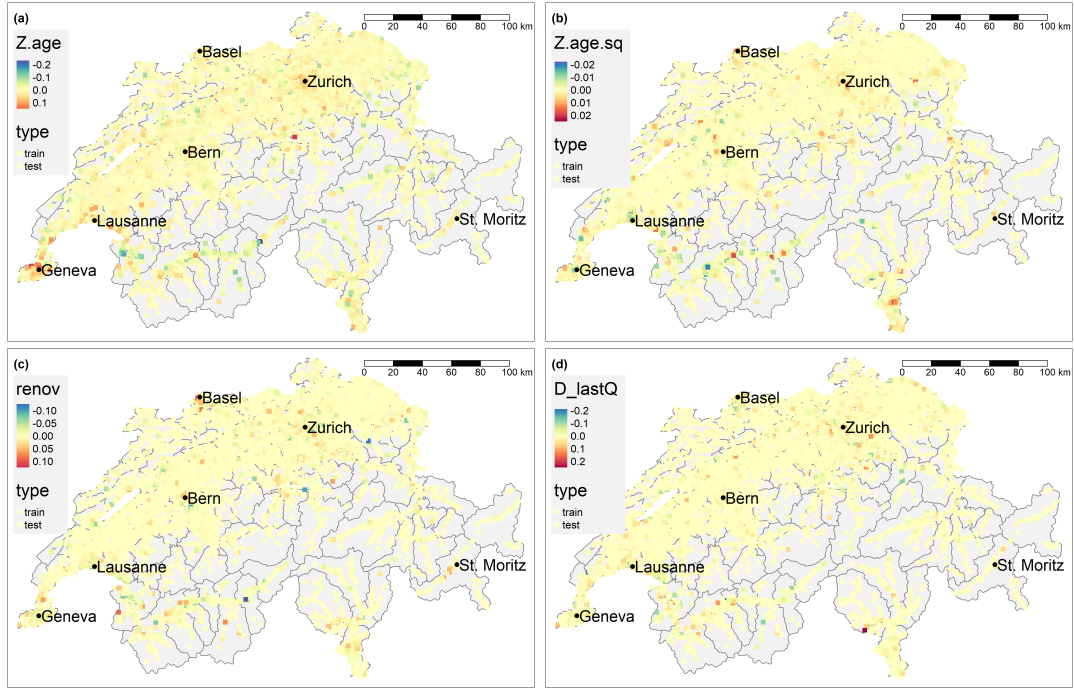


Figure 16: ML-estimated, further SVCs of the model (11) using MLE.r as defined in this Section 6. These estimated SVCs are supplementary to the ones depicted in Figure 6. This figure shows (a) $\hat{\eta}_3$ for covariate `Z.age`, (b) $\hat{\eta}_4$ for covariate `Z.age2`, (c) $\hat{\eta}_7$ for covariate `renov`, and (d) $\hat{\eta}_8$ for covariate `DlastQ`. The squares indicate training locations $\mathcal{S}_{\text{train},1}$, the dots are extrapolations to all other centroids.